AD_____

Award Number: DAMD17-99-1-9069

TITLE: Mouse Mammary Cancer Models - Mechanisms and Markers

PRINCIPAL INVESTIGATOR: Lawrence A. Donehower, Ph.D.

CONTRACTING ORGANIZATION: Baylor College of Medicine
Houston, Texas 77030

REPORT DATE: August 2002

TYPE OF REPORT: Annual Summary

PREPARED FOR: U.S. Army Medical Research and Materiel Command
Fort Detrick, Maryland 21702-5012

DISTRIBUTION STATEMENT: Approved for Public Release;
Distribution Unlimited

REPORT DOCUMENTATION PAGE

Form Approved
OMB No. 074-0188

1. AGENCY USE ONLY (Leave blank)	2. REPORT DATE	3. REPORT TYPE AND DATES COVERED
	August 2002	Annual Summary (1 Aug 99 - 31 Jul 02)

4. TITLE AND SUBTITLE
Mouse Mammary Cancer Models - Mechanisms and Markers

5. FUNDING NUMBERS
DAMD17-99-1-9069

6. AUTHOR(S)
Lawrence A. Donehower, Ph.D.

7. PERFORMING ORGANIZATION NAME(S) AND ADDRESS(ES)
Baylor College of Medicine
Houston, Texas 77030

E-Mail: larryd@bcm.tmc.edu

8. PERFORMING ORGANIZATION REPORT NUMBER

9. SPONSORING / MONITORING AGENCY NAME(S) AND ADDRESS(ES)
U.S. Army Medical Research and Materiel Command
Fort Detrick, Maryland 21702-5012

10. SPONSORING / MONITORING AGENCY REPORT NUMBER

11. SUPPLEMENTARY NOTES
report contains color

12a. DISTRIBUTION / AVAILABILITY STATEMENT
Approved for Public Release; Distribution Unlimited

12b. DISTRIBUTION CODE

13. Abstract ***(Maximum 200 Words)*** *(abstract should contain no proprietary or confidential information)*

We have generated and characterized several mouse models to better understand the role of breast cancer associated genes in an experimentally manipulable context. We have focused on the role of p53 and p53 target genes and their role in promoting mammary cancer. Recent emphasis has been placed on the Wild type p53-Induced Phosphatase (Wip1), also known as Ppm1D. This gene has recently been demonstrated to be an oncogene in vitro and to be specifically amplified in more than 15% of human breast cancers. To study the role of Wip1 in mammalian development, physiology, and cell cycle control, we generated knockout mice that are deficient in Wip1. Wip1-deficient mice exhibit multiple developmental defects and their cells show defects in cell cycle progression. We have confirmed that Wip1 is radiation-induced p53 target gene and we have identified three novel potential Wip1 interacting proteins.

14. SUBJECT TERMS
breast cancer, p53, Wip1

15. NUMBER OF PAGES
23

16. PRICE CODE

17. SECURITY CLASSIFICATION OF REPORT	18. SECURITY CLASSIFICATION OF THIS PAGE	19. SECURITY CLASSIFICATION OF ABSTRACT	20. LIMITATION OF ABSTRACT
Unclassified	Unclassified	Unclassified	Unlimited

Table of Contents

INTRODUCTION:

The p53 tumor suppressor gene is a critical stress response gene that is mutated in 30-40% of all human breast cancers (1). In those breast cancers where p53 is not structurally altered, it may be functionally inactivated through alterations in p53 signaling (1). The overall goals of this Academic Award have been to understand the mechanistic role of p53 loss or mutation in mammary tumorigenesis and to identify markers and targets of p53 that may be altered in the tumorigenic process.

During the final year of this Academic Award, we have focused on one particular p53 target gene that has recently emerged as an important player in a significant percent of human breast cancers. The Wip1 gene, also known as Ppm1d, encodes a p53-induced phosphatase (2), and is specifically amplified in 20% or more of all human breast cancers (3,4). Wip1 also has transforming activity in in vitro transformation assays, indicating that it may be a bona fide human oncogene (3,4). Wip1 may downregulate p53 activity through dephosphorylation of p38 MAP kinase (5). Thus, its overexpression may functionally inactivate p53 and promote tumor formation.

To further study the role of Wip1 in mammary tumorigenesis models, we have isolated the murine Wip1 cDNA and genomic DNA and have generated Wip1 knockout mice. Wip1 knockout mice show a number of developmental and physiological defects, and embryo fibroblasts derived from them display defects in cell cycle progression. Through two hybrid approaches, we have also identified two Wip1 interacting proteins. These proteins are critical DNA repair proteins, thus providing new clues into the role of Wip1 in cell signaling pathways.

RESEARCH ACCOMPLISHMENTS:

1. The murine *Wip1* gene

In 1997, we began a collaboration with Dr. Ettore Appella, the discoverer of the human *Wip1* gene (2). We initiated a mouse knockout strategy after obtaining the human *Wip1* cDNA clone from Dr. Appella. A 129/Sv mouse genomic lambda phage library was screened with the human *Wip1* cDNA and multiple *Wip1* positive clones were isolated (6). In addition, *Wip1* cDNA clones were isolated from commercially available murine cDNA libraries. Sequence analysis of the cDNAs and appropriate regions of the genomic clones allowed assembly of the murine *Wip1* coding sequences as well as intron-exon junctions, non-coding transcribed sequences and the upstream promoter region (6). The *Wip1* coding sequence is 598 amino acids, which closely agrees with the human *Wip1* of 605 amino acids. The mouse *Wip1* sequence has an overall identity of 83% with human *Wip1* at the amino acid level. Moreover, there are several large regions with 100% identity, including large regions of the evolutionarily conserved type 2C phosphatase domain. Several domains of the murine *Wip1* gene are conserved with PP2C phosphatases from yeast, flies, plants, and humans (6).

Since initial sequencing of the *Wip1* promoter did not reveal a p53 response element, we wanted to confirm that *Wip1* was a p53 responsive gene in an *in vivo* context. We irradiated p53+/+ and p53-/- mice with 10 Gy of ionizing radiation and sacrificed them six hours later. Semi-quantitative RT-PCR with *Wip1*, p21, and actin-specific primers was performed on total RNA from spleen, kidney, and testis of p53+/+ and p53-/- mice. The results indicated that, like the p53 responsive gene p21, *Wip1* RNA expression levels are increased in p53+/+ tissues, but not p53-/- tissues (Figure 1) (7). This data supports previous *in vitro* data that *Wip1* is indeed a p53-induced gene.

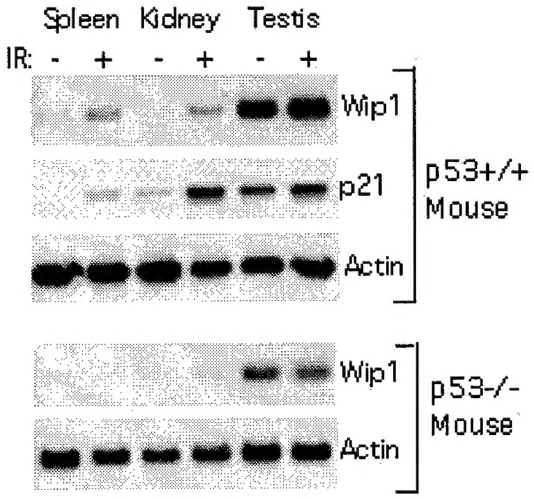

Figure 1. p53 induction of Wip1 in mouse tissues following ionizing radiation (IR) treatment. RT-PCR assay on RNAs isolated from spleen, kidney, and testis of unirradiated and IR-treated p53+/+ and p53-/- mice (10 Gy, 6 hr).

2. The *Wip1*-deficient mouse

With*Wip1* genomic clones from a 129/Sv library we constructed a *Wip1* gene targeting vector to inactivate *Wip1* in embryonic stem (ES) cells. This targeting vector replaces highly conserved exons 4 and 5 of *Wip1* with a Puro selection cassette. This deletion eliminates critical regions of the phosphatase domain. Using standard methods, chimeric mice were generated and F1 mice that transmitted the mutant *Wip1* allele were crossed to generate *Wip1*-/- mice. Only 16% of the offspring of *Wip1*+/- parents were *Wip1*-/-, suggesting a possible embryonic selection against null fetuses. *Wip1*-/- animals expressed no intact *Wip1* mRNA and protein (7).

While *Wip1*+/- animals and *Wip1*-/- females appeared morphologically normal after birth and into adulthood, the *Wip1*-/- males exhibited a variable runting phenotype (7). Mean body weight of adult *Wip1*-/- males was 21.6 grams versus 28.1 grams for *Wip1*+/+ males. Pathological examination revealed that *Wip1*-/- null animals often had smaller reproductive organs. This was particularly true of the testes (Figure 2A). This reduction in reproductive organ mass in the Wip1 males resulted in greatly reduced fertility. Histopathological examination of the null testes showed extensive degeneration of the seminiferous tubules, with vacuolization and loss of normal architecture (Figure 2B). In many tubules, there were few or no mature spermatozoa. However, there were clearly round and elongating spermatids, confirming that they had undergone meiosis and initiated terminal differentiation. The reduced fertility of the null males is likely to be a direct result of the result of reduced sperm production and storage.

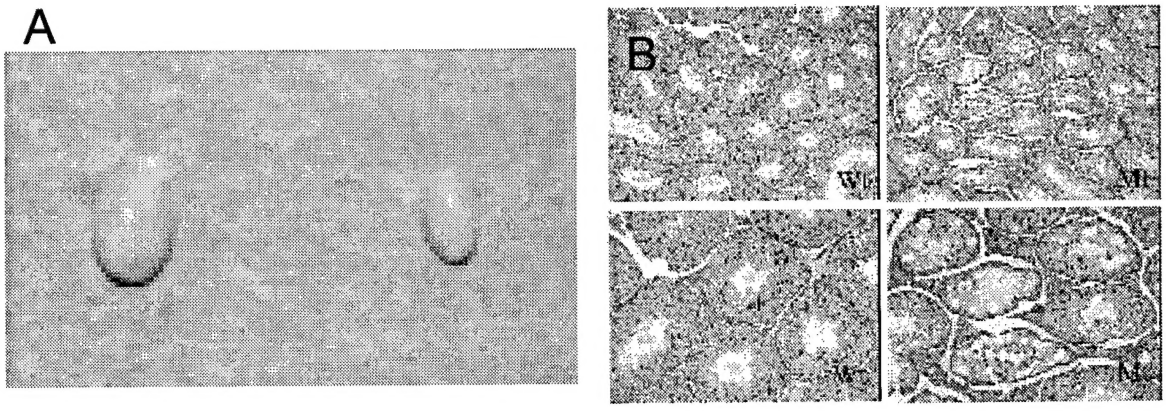

Figure 2. Abnormal testicular structure in *Wip1*-/- males. (A) Testis of *Wip1*+/+ mouse (left) and *Wip1*-/- mouse (right). (B) Testis cross sections viewed at low (top) and high (bottom) magnification from *Wip1*+/+ (left) and *Wip1*-/- (right) mice.

As the *Wip1* null mice were aged, they showed phenotypes that were not observed in the *Wip1*+/- and *Wip1*+/+ animals. Ulcerated skin lesions were observed in some of the *Wip1*-/- mice, and about 25% of older null animals of both sexes exhibited fluid filled neck abscesses (7). These conditions suggested a potential immune defect in the *Wip1* null mice. Consistent with this, the spleens of 8-11 month old *Wip1* mice showed a number of defects, including myeloid and plasmacytic hyperplasia. In some cases the splenic hyperplasia was accompanied by loss of normal splenic architecture, with reduction in white pulp due to infiltration of other cell types (3). The lymph nodes and thymi of older *Wip1*-/- mice were also abnormal, with a reduction in size and a loss of normal medullary-cortical architecture. A number of organs in the *Wip1* null mice exhibited high levels of inflammation (7).

The above phenotypes suggested that the *Wip1*-/- mice had immune defects. To determine whether the *Wip1* null mice had reduced immunity, we challenged them (and *Wip1*+/- controls) with one LD50 dose of mouse-adapted pathogenic influenza virus obtained from our collaborator, Dr. Innocent Mbawuike. All of the infected mice showed a high degree of morbidity and body weight loss by 7 days post-infection. However, all four *Wip1* null mice had died by 11 days post-infection, while four of five *Wip1*+/- mice recovered from the virus and survived (Figure 3A) (7). This survival difference was significant and indicates that *Wip1* null mice do have a bona fide immune deficiency. To determine whether T and B cell function is affected, we harvested fresh spleen cells from 3-6 month old *Wip1*+/+ and *Wip1*-/- mice and measured their proliferative response to mitogenic stimulation. Stimulation of the T cell receptor with anti-CD3 and anti-CD28 elicited a reduced proliferative response in the *Wip1*-/- T cells compared to their *Wip1*+/+ counterparts. Moreover, stimulation of spleen cells with the T-cell mitogen PHA or the B cell mitogen LPS also showed a defective response in the *Wip1*-/- T and B cells, respectively (Figure 3B,C) (7).

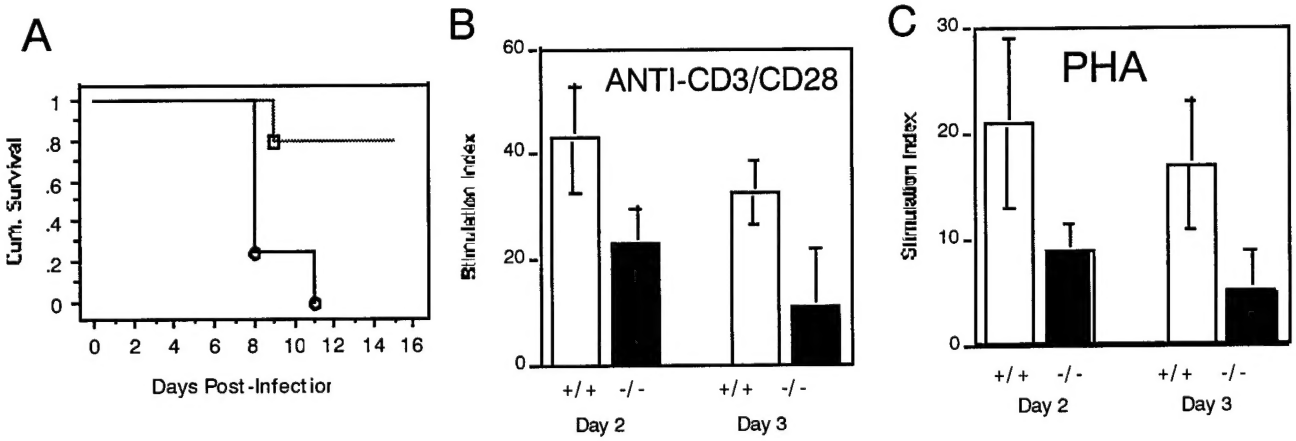

Figure 3. Evidence of immune deficiencies in *Wip1*-/- mice. (A) Survival of 5 *Wip1*+/- males (rectangles) and 4 *Wip1*-/- males (circles) following inoculation of one LD50 dose of mouse-adapted influenza virus at day 0. (B) *Wip1*+/+ and *Wip1*-/- T-cell proliferative responses to T-cell receptor stimulation. (C) *Wip1*+/+ and *Wip1*-/- T-cell proliferative responses to mitogen stimulation.

We aged cohorts of *Wip1*-/-, *Wip1*+/-, and *Wip1*+/+ mice for 24 months to monitor for longevity and aging-associated diseases such as cancer. Surprisingly, there was a dramatic sex-specific difference in longevity between the *Wip1* null males and females. Only 3 of 20 *Wip1*-/- males survived to 24 months, while 15 of 17 *Wip1*-/- females lived to two years of age, which was similar to the longevity profiles of *Wip1*+/- and *Wip1*+/+

animals of both sexes (Figure 4) (7). We have yet to observe any overt tumors in the *Wip1*-/- animals, unlike their wild type counterparts, 50% of which succumb to tumors around the age of two years. If real, such tumor resistance in the *Wip1* null animals would be consistent with a more activated p53. We have previously observed mice with apparent hyperactive p53 that were also highly cancer resistant (8).

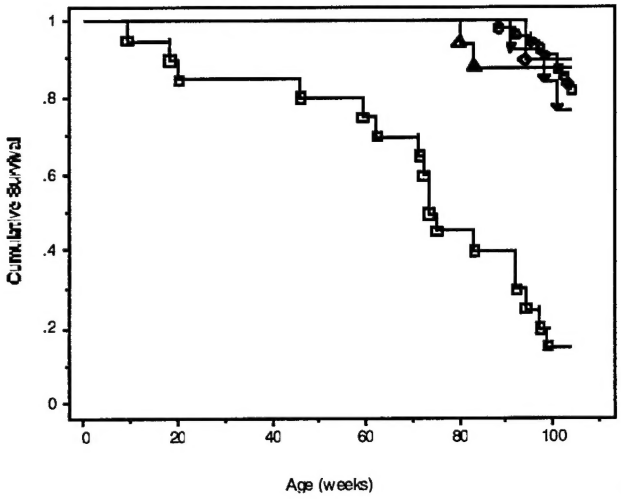

Figure 4. Decreased longevity in Wip1-/- male mice. Kaplan-Meier survival plots of Wip1-/- males (squares , n = 20), Wip1-/- females (triangles, n = 17), Wip+/- males (diamonds, n =10), Wip1+/- females (inverted triangles (n = 13), and Wip1+/+ mice (circles, n = 55).

3. Properties of *Wip1*-deficient embryo fibroblasts

The potential ability of Wip1 to regulate p53 and thus affect cell cycle control led us to examine the growth phenotypes of fibroblasts derived from *Wip1*-/- mice and *Wip1*+/+ midgestation embryos. *Wip1*-/- mouse embryo fibroblasts (MEFs) exhibited decreased growth rates in culture compared to their *Wip1*+/+ counterparts (Figure 5A) (7). Flow cytometric analyses indicated that *Wip1*-/- MEFs had a delayed cell cycle progression with an apparent block in G2/M. Three times as many *Wip1*+/+ MEFs were in mitosis compared to *Wip1*-/- MEFs, suggesting a block in mitotic entry by the *Wip1*-/- cells. Long term passaging of *Wip1* null cells showed that by passage 5 *Wip1*-/- cells grew slowly and exhibited phenotypes associated with senescent cells (Figure 5B) (7).

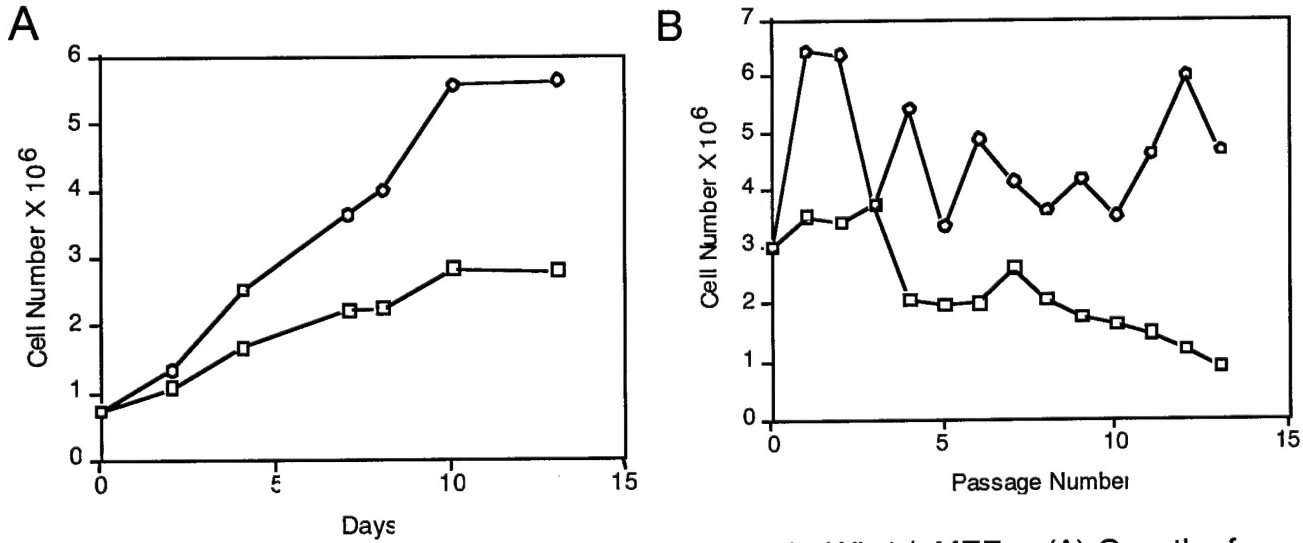

Figure 5. Reduced growth rates and early senescence in *Wip1*-/- MEFs. (A) Growth of 7.5 X 10^6 early passage MEFs derived from *Wip1*+/+ (circles) and *Wip1*-/- (squares) embryos. (B) Long-term passaging of *Wip1*+/+ (circles) and *Wip1*-/- (squares) MEFs.

To examine G1 arrest, we treated *Wip1*+/+, *Wip1*-/-, and p53-/- MEFs with 5 Gy of ionizing radiation, followed by BrdU incubation and analysis of S phase entry by BrdU incorporation. The *Wip1*-/- MEFs consistently showed a more robust G1 arrest than did *Wip1*+/+ MEFs (7). Loss of the negative feedback loop provided by *Wip1* might thus keep p53 in a more activated state for a longer time. To test this, we examined p53 protein levels, p53 serine phosphorylation, and p21 protein, all markers for increased p53 activity, in early passage *Wip1*-/- and *Wip1*+/+ MEFs. While p53 protein levels were similar, serine 15 phosphorylation of p53 and p21 levels were consistently increased in *Wip1* null cells compared to wild type cells (Figure 6) (7). Thus, absence of *Wip1* appears to decrease cell growth rates, cell cycle progression, predispose to early senescence, increase cell cycle arrest following DNA damaging agents, and increase p53 activity levels. This result is consistent with the absence of tumors observed in the *Wip1* null mice and also suggests the possibility that overexpression of Wip1 could have the reverse effect and promote oncogenicity. This result would be consistent with the observation of amplification of *Wip1* in a fraction of human breast cancers (3,4).

Figure 6. Increased p53 activity in early passage *Wip1*-/- MEFs. (A) p53 protein levels in early passage *Wip1*+/+ and *Wip1*-/- MEFs. (B) Phosphorylation of serine 15 in *Wip1*+/+ and *Wip1*-/- MEFs as detected by an antibody specific for phosphorylated serine 15. (C) $p21^{WAF1/CIP1}$ protein levels in *Wip1*+/+ and *Wip1*-/- MEFs.

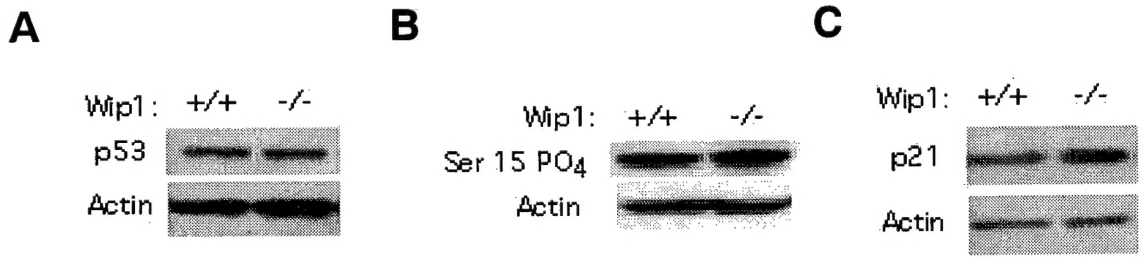

4. Wip1-interacting proteins

A phosphatase such as Wip1 is likely to have a number of phosphorylated target substrates. As an initial step to identify Wip1 interactors, we have begun bacterial two hybrid assays using the BacterioMatch Two-Hybrid System from Stratagene. So far, we have identified two genes of known function. These are the regulatory subunit of DNA polymerase delta and the repair enzyme uracil DNA glycosylase (identified in two independent clones). Both of these enzymes are key players in DNA repair (9,10). Uracil DNA glycosylase initiates the process of base excision repair by hydrolyzing an inappropriate uracil base from the deoxyribose. After endonucleolytic excision of the modified deoxyribose, the correct nucleotides can be inserted by a repair polymerase such as DNA polymerase beta or delta. DNA polymerase delta is also important for DNA mismatch repair and nucleotide excision repair and mice with inactivated DNA polymerase delta are highly susceptible to early tumors (11). The identification of two enzymes involved in base excision repair by the two hybrid method strongly suggests that Wip1 might be regulating this repair process and possibly other types of DNA repair. Since p53 regulates base excision repair, we can envision a hypothetical model in which DNA damage causes activated p53, which in turn stimulates base excision repair activity. Meanwhile p53 also activiates transcription of Wip1 and accumulating Wip1 protein eventually facilitates deactivation of p53 through p38 MAP kinase, and may also dephosphorylate base excision repair components such as uracil DNA glycosylase and return these proteins to basal non-stressed levels of activity.

LIST OF KEY RESEARCH ACCOMPLISHMENTS

(1) Generation and characterization of Wip1 knockout mice and publication of the results in Molecular and Cellular Biology.

(2) Elucidation of altered immune, reproductive, and longevity phenotypes in Wip1 null mice.

(3) Demonstration that cells derived from Wip1 null mice are defective for aspects of cell cycle progression.

(4) Identification of novel Wip1 interacting proteins that are involved in DNA repair.

LIST OF REPORTABLE OUTCOMES:

1. Choi J, Nannenga B, Demidov O, Bulavin D, Cooney A, Brayton C, Zhang Y, Mbawuike IN, Bradley A, Appella E, Donehower LA. 2002. Mice deficient for the wild type p53-induced phosphatase gene (*Wip1*) exhibit defects in reproductive organs, immune function, and cell cycle control. Mol. Cell. Biol 22:1094-1105.

CONCLUSIONS:

1. Wip1 is a p53-induced phosphatase that is highly conserved among mammals and is specifically amplified in over 20% of human breast cancers.

2. Wip1 null mice exhibit multiple defects in growth, reproductive function, immune function, and longevity, indicating that Wip1 is a gene that plays an important role in many organismal physiological functions.

3. Embryo fibroblasts from Wip1 null mice show alterations in enhanced G1 arrest function, defective mitotic entry, reduced growth rates, and increased activity of p53. This is consistent with a role for Wip1 in inactivation of p53 by a negative feedback loop mechanism.

4. Wip1 appears to play a role in DNA repair as evidenced by its interaction with two DNA repair proteins. This further suggests a link with p53 signaling to alterations in DNA repair function.

REFERENCES:

1. Olivier M, Hainaut P. 2001. TP53 mutation patterns in breast cancers: searching for clues of environmental carcinogenesis. Semin Cancer Biol. 11:353-360.

2. Fiscella M, Zhang H, Fan H, Sakaguchi K, Shen S, Mercer WE, Vande Woude GF, O-Connor PM, Appella E. 1997. Wip1, a novel human protein phosphatase that is induced in response to ionizing radiation in a p53-dependent manner. Proc. Natl. Acad. Sci. USA 94:6048-6053.

3. Bulavin DV, Demidov ON, Saito S, Kauraniemi P, Phillips C, Amundson SA, Ambrosino C, Sauter G, Nebreda AR, Ancerson CW, Kallioniemi A, Fornace Jr. AJ, Appella E. 2002. Amplification of the Wip1 phosphatase gene in human tumors abrogates p53 tumor-suppressor activity. Nature Genet. 31:210-215.

4. Li J, Yang Y, Peng Y, Austin RJ, van Eyndhoven WG, Nguyen KCQ, Gabriele T, McCurrach ME, Marks JR, Hoey T, Lowe SW, Powers S. 2002. Oncogenic properties of PPM1D located within a breast cancer amplification epicenter at 17q23. Nature Genet. 31:133-134.

5. Takekawa M, Adachi M, Nakahata A, Nakayama I, Itoh F, Tsukuda H, Taya Y, Imai K. 2000. p53-inducible wip1 phosphatase mediates a negative feedback regulation of p38 MAPK-p53 signaling in response to UV radiation. EMBO J. 19:6517-6526.

6. Choi J, Appella E, Donehower LA. 2000. The structure and expression of the murine wild-type p53-induced phosphatase (Wip1) gene. Genomics 64:298-306.

7. Choi J, Nannenga B, Demidov O, Bulavin D, Cooney A, Brayton C, Zhang Y, Mbawuike IN, Bradley A, Appella E, Donehower LA. 2002. Mice deficient for the wild type p53-induced phosphatase gene (*Wip1*) exhibit defects in reproductive organs, immune function, and cell cycle control. Mol. Cell. Biol 22:1094-1105.

8. Tyner SD, Venkatachalam S, Choi J, Jones SM, Ghebranious N, Igelmann H, Lu X, Soron G, Cooper B, Brayton C, Park SH, Thompson T, Karsenty G, Bradley A, Donehower LA. 2002. p53 mutant mice that display early aging associated phenotypes. Nature 415:45-53.

9. Hoeijmakers JJ. 2001. Genome maintenance mechanisms for preventing cancer. Nature 411:366-374.

10. Nilsen H, Krokan HE. 2001. Base excision repair in a network of defence and tolerance. Carcinogenesis 22:987-998.

11. Goldsby RE, Lawrence NA, Hays LE, Olmsted EA, Chen X, Singh M, Preston BD. 2001. Defective DNA polymerase-delta proofreading causes cancer susceptibility in mice. Nat Med. 7:638-639.

MOLECULAR AND CELLULAR BIOLOGY, Feb. 2002, p. 1094–1105 Vol. 22, No. 4
0270-7306/02/$04.00+0 DOI: 10.1128/MCB.22.4.1094–1105.2002

Mice Deficient for the Wild-Type p53-Induced Phosphatase Gene (*Wip1*) Exhibit Defects in Reproductive Organs, Immune Function, and Cell Cycle Control

Jene Choi,[1,2] Bonnie Nannenga,[3] Oleg N. Demidov,[4] Dmitry V. Bulavin,[4] Austin Cooney,[3] Cory Brayton,[5] Yongxin Zhang,[1] Innocent N. Mbawuike,[1] Allan Bradley,[6,7] Ettore Appella,[4] and Lawrence A. Donehower[1,3]*

Department of Molecular Virology and Microbiology,[1] Department of Molecular and Cellular Biology,[3] Center for Comparative Medicine,[5] and Department of Molecular and Human Genetics,[6] Baylor College of Medicine, Houston, Texas 77030; Department of Pathology, University of Ulsan College of Medicine, Asan Medical Center, Seoul, Korea[2]; Laboratory of Cell Biology, Division of Basic Sciences, National Cancer Institute, National Institutes of Health, Bethesda, Maryland 20892[4]; and The Sanger Centre, Wellcome Trust Genome Campus, Cambridgeshire CB10 1SA, United Kingdom[7]

Received 8 August 2001/Returned for modification 3 October 2001/Accepted 12 November 2001

The *Wip1* gene is a serine/threonine phosphatase that is induced in a p53-dependent manner by DNA-damaging agents. We show here that *Wip1* message is expressed in moderate levels in all organs, but is present at very high levels in the testes, particularly in the postmeiotic round spermatid compartment of the seminiferous tubules. We have confirmed that *Wip1* mRNA is induced by ionizing radiation in mouse tissues in a p53-dependent manner. To further determine the normal biological function of Wip1 in mammalian organisms, we have generated *Wip1*-deficient mice. *Wip1* null mice are viable but show a variety of postnatal abnormalities, including variable male runting, male reproductive organ atrophy, reduced male fertility, and reduced male longevity. Mice lacking *Wip1* show increased susceptibility to pathogens and diminished T- and B-cell function. Fibroblasts derived from *Wip1* null embryos have decreased proliferation rates and appear to be compromised in entering mitosis. The data are consistent with an important role for Wip1 in spermatogenesis, lymphoid cell function, and cell cycle regulation.

The p53 tumor suppressor protein plays a critical role in integration of signals that regulate cell growth and death in response to a variety of stressors (11, 12, 26). Loss or mutation of the gene encoding the p53 protein predisposes a cell to neoplastic transformation (8, 21, 23). Mutation of the p53 gene has been observed in half of all human cancers, and loss of p53 signaling may play a role in over 80% of all tumors (8, 12, 13).

In response to a variety of cell stresses, including DNA damage, aberrantly activated oncogenes, and hypoxia, p53 is phosphorylated on multiple serine and threonine residues, becomes stabilized, and accumulates in the nucleus (11, 12, 26). The activated p53 protein is a transcription factor that can upregulate as well as downregulate a battery of genes which participate in the biological response to the cell stress. This response can be in the form of cell cycle arrest, apoptosis, differentiation, or senescence. Any of these responses are likely to prevent the outgrowth of a nascent cancer cell.

Among the many p53 transcriptional targets that have recently been identified is the wild-type p53-induced phosphatase (Wip1) (5). The *Wip1* gene exhibits a close similarity to type 2C phosphatases (2, 5). The type 2C phosphatases are distinguished from the PP1, PP2A, and PP2B phosphatases by their insensitivity to phosphatase inhibitors such as okadaic acid and requirement for divalent cations (Mg^{2+} or Mn^{2+}) (3, 15). The type 2C phosphatases have been identified in a wide range of organisms and have often been associated with stress response, sexual differentiation, and cell cycle control (3, 15).

The *Wip1* gene was originally identified in a screen for p53 target genes (5). Wip1 was shown to be upregulated in a p53-dependent manner by ionizing radiation (IR) and by UV radiation (UV) (5, 25). Following IR, *Wip1* mRNA was rapidly induced and the protein was localized to the nucleus. The first specific target of the Wip1 phosphatase has recently been shown by Takekawa et al. (25) to be the p38 mitogen-activated protein (MAP) kinase protein. Phosphorylation of p38 is directly inhibited by Wip1. UV irradiation of cells causes rapid phosphorylation of a serine and threonine residue on p38, which activates its kinase activity. In turn, activated p38 MAP kinase can phosphorylate p53 on residues Ser33 and Ser46 in response to UV damage. UV-induced phosphorylation of p53 by p38 is associated with increased p53 transcriptional activity and apoptosis induction. Takekawa et al. (25) have shown that Wip1 selectively inhibits p38 through dephosphorylation of an activation-associated threonine residue. This results in downregulation of phosphorylation on UV-responsive p53 Ser33 and Ser46 residues. These data suggest that Wip1 may be a mediator of a negative feedback loop for p53 following its UV-induced activation.

Given the emerging relevance of Wip1 in p53-mediated cell cycle control and DNA damage response, we have begun to investigate the biological functions of Wip1 through studies of its activity in the mouse. In this paper, we confirm that Wip1 is activated by IR in a p53-dependent manner in multiple tissues of the mouse. We demonstrate that *Wip1* mRNA is ubiquitously expressed, though at particularly high levels in the post-

* Corresponding author. Mailing address: Department of Molecular Virology and Microbiology, Baylor College of Medicine, One Baylor Plaza, Houston, TX 77030. Phone: (713) 798-3594. Fax: (713) 798-3490. E-mail: larryd@bcm.tmc.edu.

meiotic round spermatid compartment of the testes. We have also generated *Wip1* null mice through gene targeting techniques and show that while such mice appear to exhibit normal embryonic development, they show defects in growth, organ structure, fertility, and lymphoid function. Embryo fibroblasts deficient for *Wip1* show multiple defects in cell cycle control. All of these organismal and cellular phenotypes indicate that Wip1 does play an important role in the regulation of cell growth and in the function of a number of adult organ systems.

MATERIALS AND METHODS

RNA analyses. For Northern blot analyses of *Wip1* mRNA, tissues were harvested and homogenized with a Polytron homogenizer in Trizol buffer reagent (Life Technologies), followed by purification of total RNA with the Trizol RNA purification kit according to the manufacturer's specifications. Ten micrograms of total RNA from each tissue was heated to 65°C and then loaded onto a formaldehyde-agarose gel and subjected to electrophoresis as previously described (20). Northern blot hybridization was done with the Ambion NorthernMax kit according to the manufacturer's directions with a *Wip1* cDNA probe labeled with ^{32}P by random primed oligonucleotides (Roche High Prime kit). After rinsing of the blot, hybridizing bands were visualized following autoradiography on Kodak AR-5 X-ray film for 1 to 5 days.

For reverse transcription (RT)-PCR of *Wip1* RNA, $Wip1^{+/+}$ and $Wip1^{-/-}$ spleens, kidneys, and testes from irradiated and unirradiated mice were isolated and total RNA was prepared from them as described above. RT-PCR on the isolated total RNAs was performed with the SuperScript preamplification system (Gibco-BRL) according to the manufacturer's protocol. Primers used for RT-PCR were primer 1 (*Wip1*-exon 1 sense; 5′-GCCCGCCAAGGTGTGCGCTG-3′), primer 2 (*Wip1*-exon 3 antisense; 5′-CAGGTCCACTGTGAGTGAGC-3′), primer 3 (*Wip1*-exon 3 sense; 5′-TCACTCACAGTGGACCTG-3′), primer 4 (*Wip1*-exon 6 antisense; 5′-AGGGCAGGTATATGGTCCTTAGA-3′), and primer 5 (*Wip1*-exon 4 sense; 5′-AGTGATGGACTTTGGAATAT-3′).

In situ hybridization of testes sections from $Wip1^{+/+}$ and $Wip1^{-/-}$ mice was performed essentially as described previously by Choi et al. (2).

ES cell targeting. The targeting construct was generated from a murine genomic *Wip1* clone derived from a 129/Sv phage genomic library as previously described (2). The 5′ homology arm of the construct was derived from a 3.2-kb *Nhe*I fragment located between exons 3 and 4 of the *Wip1* gene. The 3′ homology arm of the targeting construct was derived from an intron 5 2.2-kb *Bam*HI segment. Between these two homology arms was placed a PGK-Puro selectable marker cassette. Successful homologous recombination of the targeting construct and the endogenous *Wip1* allele results in deletion of all of exons 4 and 5, resulting in a severely truncated Wip1 protein. A negative selectable marker, MC1-TK, was located adjacent to the 5′ homology region.

The targeting construct was electroporated into AB1 embryonic stem (ES) cells, and puromycin-resistant, 1-(2-deoxy,2-fluoro-β-D-arabinofuranosyl)-5-iodouracil (FIAU)-resistant colonies were selected. Resistant colonies were amplified, and DNA was prepared from them and screened by Southern blot procedures as previously described (16, 17). Probes derived from genomic *Wip1* sequences upstream and downstream of the original targeting construct were used to screen for correctly targeted clones. One clone generated fragments of the expected sizes for successful homologous recombination, and this clone was further amplified and injected into 3.5-day blastocysts to generate chimeric offspring as previously described (17).

Chimeric offspring were then mated to C57BL/6 mice homozygous for a spontaneous tyrosinase gene mutation. These C57BL/6 mice were albino, so that any agouti offspring of the chimeric crosses were then analyzed for transmission of the mutant *Wip1* allele. Genotyping for mutant and wild-type *Wip1* alleles was performed by removing a 1-cm segment of the tail of weanling mice, extracting tail DNA, cleaving it with *Nco*RI, and performing agarose gel electrophoresis and Southern blot hybridization as previously described (16). The genotyping probe was a 2.2-kb *Bam*HI fragment derived from intron 5. Mutant *Wip1* alleles generated a 10-kb fragment, while the wild-type *Wip1* allele generated a 7-kb fragment.

Synthetic peptides and generation of polyclonal antibodies. A Wip1 peptide corresponding to the mouse sequence containing amino acids 20 through 60 (APVPRRALGLPATPTLAGVGP) was synthesized by the solid-phase method with Fmol chemistry using an Applied Biosystems 430A peptide synthesizer (Foster City, Calif.). The peptide after cleavage from the resin and removal of the side chain protecting groups was incubated in reagent K (trifluoroacetic acid-phenol-thioanisole-H_2O-EDTA, 82.5:5:5:5:2.5) for 3 h at room temperature and purified by high-pressure liquid chromatography (HPLC) on a pH-stable Vydac C-8 column (Hesperia, Calif.) with 0.05% trifluoroacetic acid-water-acetonitrile. The mass of the peptide was confirmed by electrospray ionization mass spectrometry on a Finnigan MAT SSQ 7000 (Finnigan MAT, San Jose, Calif.). Rabbit polyclonal antibodies were raised against the mouse Wip1 peptide coupled to keyhole limpet hemocyanin. The antibodies were affinity purified from the resulting serum by use of the peptide coupled with Sulfolink (Pierce), and the specificity of the antibody was confirmed by enzyme-linked immunosorbent assay (ELISA) and immunoblot assays.

Induction of DNA damage and Western immunoblot analysis. BALB/c and $Wip1^{-/-}$ knockout mice were irradiated with 10 Gy generated from a ^{137}Cs Shepherd Mark II irradiator. One day after irradiation, they were euthanized, and the whole testis was homogenized with a glass homogenizer. Homogenized testes or mouse embryo fibroblasts were extracted in 20 mM Tris (pH 7.5)–150 mM NaCl–0.1% Triton X-100–1 mM EDTA and a proteinase inhibitor cocktail (Roche). The extracts were then precipitated with acetone, pelleted, redissolved in sodium dodecyl sulfate (SDS) sample buffer, boiled, separated on an SDS–10% polyacrylamide gel electrophoresis (PAGE) gel and transferred to a polyvinylidene difluoride membrane. The membrane was blocked with 5% dry milk and probed either with a purified polyclonal antibody against Wip1 peptide, polyclonal antibody to p53 (M-19, Santa Cruz), polyclonal antibody to p21 (C-19, Santa Cruz), or a polyclonal antibody specific for a p53 phosphorylated serine 15 (Cell Signaling). The filter was subsequently incubated with horseradish peroxide-conjugated secondary antibody, developed with ECL Plus, and exposed to X-ray film. To standardize the amount of protein in each lane, the filter was stripped and probed with a polyclonal antibody against actin (Santa Cruz) and developed with ECL Plus.

Mice. After *Wip1* germ line heterozygotes were obtained, these mixed 129/Sv-C57BL/6 mice were intercrossed to obtain $Wip1^{-/-}$ offspring. $Wip1^{-/-}$, $Wip1^{+/-}$, and $Wip1^{+/+}$ offspring were monitored for disease (including cancer), body weight, fertility, and longevity over a period of 2 years in the Baylor College of Medicine vivarium. Seriously morbid mice were sacrificed and subjected to a complete necropsy. Organs were examined, weighed, and fixed in formalin in preparation for histopathology as previously described (24). Spontaneous deaths were recorded and necropsies were performed if death was recent. The experiments with mice described here complied with all relevant federal guidelines and Baylor College of Medicine policies.

Histopathology. Histopathology on organs from $Wip1^{+/+}$, $Wip1^{+/-}$, and $Wip1^{-/-}$ mice was performed by standard methods as previously described (18, 24). Hematoxylin- and eosin-stained slides were examined for histopathology by standard methods (18, 24).

Flow cytometry. For analysis of B cells, freshly isolated splenic cells were placed in phosphate-buffered saline (PBS) and stained with a mixture of fluorescein isothiocyanate (FITC)-conjugated goat anti-mouse immunoglobulin G (IgG) polyclonal antibody (Sigma Chemical Company, St. Louis, Mo.) and a phycoerythrin (PE)-conjugated monoclonal rat anti-mouse CD19 (BD Pharmingen, San Diego, Calif.). For T cells, the lymphocytes were stained with a mixture of rat anti-mouse CD4-FITC, CD8-PE, and CD3-peridinin chlorophyll protein (PerCP) (BD Pharmingen). Appropriate preimmune FITC-conjugated goat IgG and rat IgG isotype controls were also used. After incubation at room temperature for 30 min, the cells were washed and suspended in 1% paraformaldehyde. Stained cells were stored at 4°C in the dark and analyzed within 24 h using two-color or three-color flow cytometry (Epics XL MCL; Beckman Coulter, Miami, Fla.).

Susceptibility to influenza virus infection. Mice were challenged with 1 50% lethal dose (LD50) of mouse-adapted influenza A/Taiwan/1/86 (H1N1) virus using small particle aerosols as previously described (14). Briefly, mouse lung virus pools were diluted in minimal essential medium (stabilized with 0.05% gelatin) and placed in a nebulizer. Male and female mice were placed in microisolator cages covered with a Plexiglas with two vents (1 mm in diameter) and sealed on the edges with masking tape. They were then exposed to virus aerosols generated by compressed N_2 and driven via an aerosol tube into the cages. Aerosolization lasted approximately 60 min. Following exposure, the infected mice were monitored daily for body weight and survival up to 21 days.

Lymphoproliferative responses. Splenic lymphocytes were cultured at a concentration of 10^5 cells per well (96-well plate) in RPMI 1640 medium supplemented with 2 mM L-glutamine, 100 U of penicillin, 100 μg of streptomycin (JRH Biosciences, Lenexa, Kans.), 5×10^{-5} M 2-mercaptoethanol (2-ME), 10 mM HEPES buffer, and 10% heat-inactivated fetal bovine serum (FBS) per ml. T cells were stimulated with monoclonal anti-CD3 and anti-CD28 (1 μg/ml) (BD Pharmingen) or phytohemagglutinin (PHA; 2 μg/ml; Wellcome Diagnostics, Dartford, England), and B cells with lipopolysaccharide (LPS) (*Escherichia coli*

O55:B5, 10 μg/ml; Sigma). After incubation for 48 h at 37°C in a 5% CO_2 humidified air incubator, the cells were pulsed with 0.5 μCi of [^{3}H]thymidine ([^{3}H]TdR, 6.7 mCi/ml; ICN Radiochemicals, Irvine, Calif.) for 18 to 24 h and harvested on glass fiber filter mats using a semiautomatic harvester (Skatron). Radioactivity incorporation was determined using a beta scintillation counter. The stimulation index (SI) for each mitogen was obtained by dividing the mean cpm of incorporation by mean control (medium alone) cpm. Differences between mean SI among groups were determined by Student's *t* test in analysis of variance.

MEF studies. *Wip1*$^{+/-}$ adult males and females were mated and examined for vaginal plugs each morning. Twelve days after visualization of the vaginal plug, the pregnant female was sacrificed and embryo fibroblasts were prepared from each embryo as previously described (6). DNA was prepared from a small portion of each embryo, and the *Wip1* genotype was determined as described above. Several vials of passage 1 mouse embryo fibroblasts (MEFs) were frozen for each embryo.

For growth curve experiments, three lines each of *Wip1*$^{+/+}$ and *Wip1*$^{-/-}$ MEFs were thawed, plated, and counted. Procedures were those described previously (9). A total of 7.5×10^5 MEFs were plated on multiple 100-mm dishes for each line in 10% fetal calf serum and Dulbecco's modified Eagle's medium (DMEM). Two plates were then harvested, and cells were counted by hemacytometer at intervals of 2, 4, 7, 8, 10, and 13 days. Fluorescence-activated cell sorting (FACS) analysis of early-passage primary MEFs was performed by standard procedures (9).

The number of cells in S phase was counted after pulse labeling with bromodeoxyuridine (BrdU) as previously described (1). The percentage of cells in mitosis was determined by microscopic visualization after fixing and staining the cells with antiphosphohistone H3 antibody (Upstate Biotechnology). For the colony plating assay, early-passage primary MEFs were plated at low density (10,000 cells per 10-cm plate) and incubated for 2 weeks with regular changes of medium. Cell colonies (>30 cells) were then fixed, stained, and counted. Experiments were performed in triplicate.

For long-term passaging experiments, three *Wip1*$^{+/+}$ and *Wip1*$^{-/-}$ early-passage lines were used and conditions were similar to those described previously (9). One million cells of each line were plated on each of three 60-mm dishes, and every 3 days the cells were trypsinized, counted, and replated at 10^6 cells per 60-mm dish. When there were fewer than 10^6 *Wip1*$^{-/-}$ MEFs per plate, all of the cells were replated.

For G_1 arrest assays, cells were normally plated, grown to confluency, and allowed to remain confluent for 4 to 5 days. Virtually all of these cells were arrested in G_0/G_1 by flow cytometry analysis. These synchronized cells were split into two groups, radiated and unirradiated. One group was treated with 5 Gy of ionizing radiation, and one group remained unirradiated. BrdU (10 μM) was added, and the cells were plated at lower density. The cells were then harvested at 24, 48, and 72 h, fixed in 70% ethanol, and subjected to double staining for DNA content (propidium iodide staining) and BrdU incorporation (staining with FITC-conjugated anti-BrdU antibody) prior to flow cytometry. Levels of relative G_1 arrest were determined by the ratio of BrdU incorporation in the irradiated cells to the level of BrdU incorporation in the unirradiated cells for each time point.

RESULTS

***Wip1* mRNA expression in mouse testes.** Previously, we had shown that *Wip1* mRNA is expressed in all mouse tissues, but was present at very high levels in the testes (2). To ascertain whether a specific compartment of the testes shows high expression of *Wip1* mRNA, we performed in situ hybridizations with a *Wip1* probe on sections from normal adult mouse testes. *Wip1* is expressed within the cells of the seminiferous tubules (Fig. 1A and B). *Wip1* is expressed in every tubule, but its level of expression is clearly stage dependent, with highest levels of expression detected in stage 6 to 8 tubules. *Wip1* is expressed in the spermatogenic cells, with no expression detected in spermatogonia or early to mid-stage spermatocytes.

Expression of *Wip1* is first detected in the late-stage pachytene spermatocytes just prior to the completion of meiosis. Expression of the gene is maintained postmeiotically in round spermatids, with highest levels of expression in stage 6 to 8 round spermatids. The level of *Wip1* expression decreases progressively through the elongating spermatid stage. Thus, *Wip1* is expressed in spermatocytes just prior to the completion of the meiotic divisions and during round spermatid development.

To determine the onset of the high testicular expression of the *Wip1* mRNA, we performed Northern blot analyses for *Wip1* RNA levels on testes from 15-, 20-, 25-, 30-, 35-, and 40-day-old mice (Fig. 1C). Quantitation of *Wip1* mRNA normalized to glyceraldehyde-3-phosphate dehydrogenase (GAPDH) expression showed that at 15 days of age, the testes expressed very low levels of *Wip1*, but by 25 days they were expressing very high levels and these remained very high thereafter, though there was a slight dip at 30 days (Fig. 1D).

The Northern analysis shows a correlation between the onset of puberty and spermatogenesis in the mouse and the appearance of the first wave of spermatogenesis. The lack of expression of *Wip1* at day 15 is consistent with the in situ hybridization analysis in that *Wip1* is not expressed in somatic cells or early-stage spermatogenic cells, spermatogonia, and early- to mid-stage pachytene spermatocytes, which would be present at this time point. Expression of *Wip1* is only detected by day 20, when late-stage pachytene spermatocytes would be present and the first few round spermatids would populate the tubules. By day 25 most of the tubules will have undergone meiosis, leading to a large population of round spermatids, which as they elongate through day 30 leads to a decrease in *Wip1* expression. After day 30 and the completion of the first round of spermatogenesis, the next rounds initiate, leading to randomization of the spermatogenic cell populations and the steady-state level of *Wip1* expression in the testis.

p53-dependent induction of *Wip1* mRNA in mouse tissues by ionizing radiation. The *Wip1* gene was identified in a cell-based screen for p53 target genes by its p53-dependent response to ionizing radiation (5). To confirm that *Wip1* is indeed a direct target of p53 in an organismal context, we investigated *Wip1* mRNA induction in tissues of irradiated mice. p53$^{+/+}$ and p53$^{-/-}$ mice were treated with 10 Gy of ionizing radiation, and tissues were harvested 6 h later. Total RNA was prepared from spleen, kidney, and testes of the irradiated mice and subjected to semiquantitative RT-PCR with *Wip1*, p21$^{WAF1/CIP1}$ (positive control), and actin (loading control). Spleen and kidney RNA from p53$^{+/+}$ mice showed a large induction in *Wip1* and p21 levels 6 h after ionizing radiation treatment (Fig. 2). *Wip1* levels in irradiated p53$^{+/+}$ testes were only marginally increased, perhaps due to high endogenous levels of this message already present. In contrast to p53$^{+/+}$ tissues, p53$^{-/-}$ tissues showed little or no induction of *Wip1* mRNA following radiation. These data are consistent with previous cell culture studies (5, 25) and indicate that *Wip1* is induced by ionizing radiation in a p53-dependent manner both in vitro and in vivo.

Generation of a *Wip1*-deficient mouse. To understand some of the biological functions of Wip1, we initiated gene targeting of the *Wip1* gene in embryonic stem (ES) cells. To inactivate the *Wip1* gene, we designed a targeting construct in which a puromycin expression cassette replaced genomic *Wip1* sequences containing exons 4 and 5 (Fig. 3A). Exons 4 and 5 contain highly conserved sequences, and the expected targeting event would generate an allele expressing a severely truncated protein with no *Wip1* coding sequences beyond exon 3.

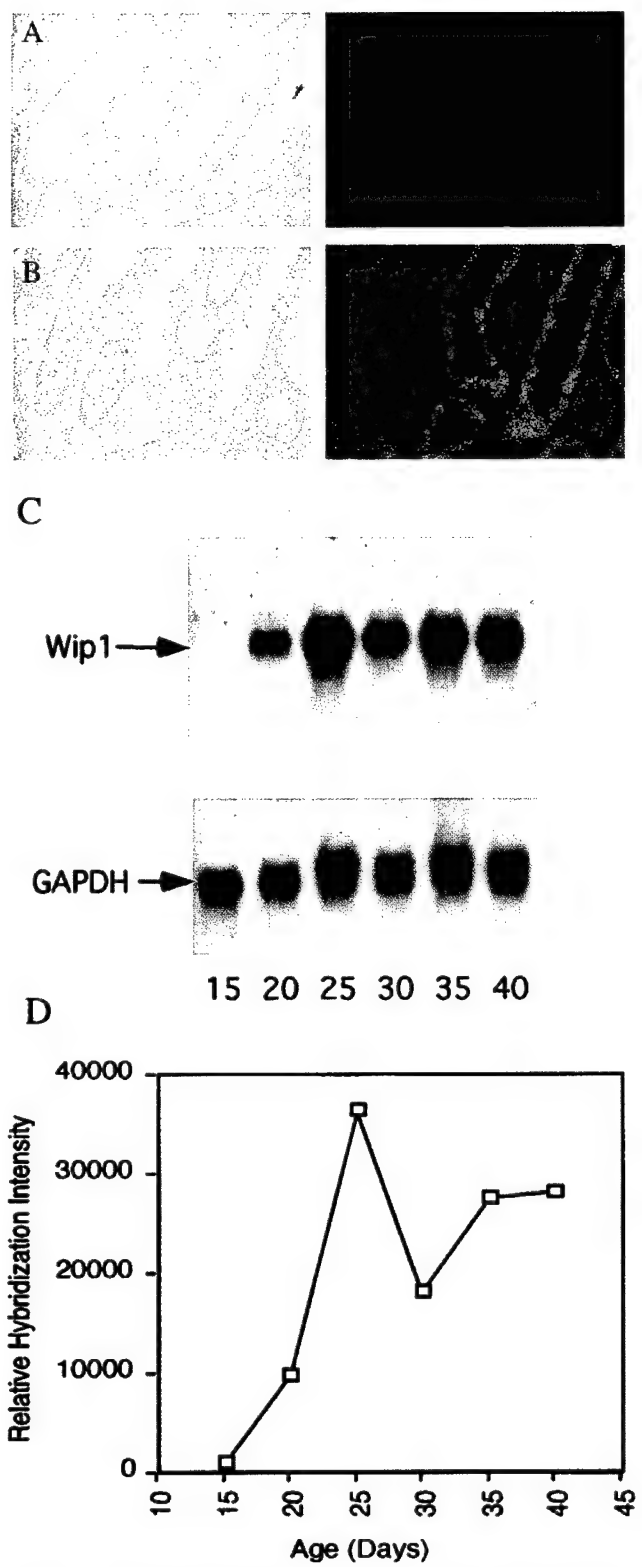

FIG. 1. *Wip1* mRNA expression in the testis. (A) Control in situ hybridization analysis of testis cross-section with the *Wip1* sense probe. The left and right panels show the light- and dark-field images, respectively, of a normal testis section following in situ hybridization. (B) In situ hybridization of testis cross-section with the *Wip1* antisense probe. The lower left and right panels show light- and dark-field images following hybridization. Note that the highest *Wip1* expression is in the postmeiotic round spermatid compartment of each of the seminiferous tubules. (C) Age-dependent changes in *Wip1* mRNA expression in the testes of male mice. Testis RNA from 15- to 40-day-old mice was analyzed by Northern blot hybridization with *Wip1* and GAPDH probes. (D) Quantitation of *Wip1* mRNA expression relative to GAPDH expression by phosphorimager analysis. Note that *Wip1* expression is initially low in the testes of 15-day-old animals but rises rapidly in the testes of 20- to 25-day-old animals.

Introduction of the targeting construct into ES cells followed by selection in puromycin (positive selection) and FIAU (negative selection) led to the identification of several clones. Restriction mapping of the *Wip1* allele in these selected clones identified one clone with the map expected after successful homologous recombination of the targeting construct and the endogenous *Wip1* allele (Fig. 3B). This clone was amplified, and standard procedures were used to reconstitute mice with a germ line mutation in the *Wip1* allele.

Germ line *Wip1* heterozygotes were crossed with each other to determine the effects of *Wip1* nullizygosity on embryonic development. In fact, while $Wip1^{-/-}$ offspring of $Wip1^{+/-}$ parents were viable at birth, there was a reduction from the expected Mendelian ratio for null pups only. Of 268 offspring of $Wip1^{+/-}$ parents, 70 (26%) were $Wip1^{+/+}$, 155 (58%) were $Wip1^{+/-}$, and only 43 (16%) were $Wip1^{-/-}$. Of the 43 $Wip1^{-/-}$ offspring, 26 were female and 17 were male, indicating a possible selection during development against male null embryos. Analysis of midgestation embryos failed to identify any obvious developmental abnormalities associated with *Wip1* nullizygosity, suggesting the possibility that a portion of $Wip1^{-/-}$ males may have early embryonic defects. However, as described below, the $Wip1^{-/-}$ males also displayed a number of postnatal defects.

To confirm the absence of intact *Wip1* expression in the *Wip1* null mice, we performed Northern blot hybridization and RT-PCR analysis on RNAs from various $Wip1^{-/-}$ tissues. Northern blot hybridization showed that the *Wip1* message was present in all of the $Wip1^{+/+}$ tissues, but was not observed at all in the $Wip1^{-/-}$ tissues (Fig. 3C). RT-PCR analysis did detect a *Wip1* message with a deletion of exons 4 and 5, but presumably this message was unstable, because even reduced-size *Wip1* mRNAs were not observed in the $Wip1^{-/-}$ lanes of the Northern blots (data not shown).

Confirmation that the $Wip1^{-/-}$ animals produce no viable Wip1 protein was provided by immunoblot analyses. Protein lysates were prepared from unirradiated and irradiated (10 Gy of IR) $Wip1^{+/+}$ testes and irradiated $Wip1^{-/-}$ testes, subjected to SDS-polyacrylamide gel electrophoresis, and immunoblotted with a Wip1 antibody specific for mouse Wip1. The irradiated $Wip1^{+/+}$ testes showed high levels of the expected 64-kDa Wip1 protein, while Wip1 of the same size was not discernible in the irradiated $Wip1^{-/-}$ testes (Fig. 3D, left panel). The same mouse antibody does not react with human Wip1, but a human-specific Wip1 antibody does react with intact 64-kDa Wip1 protein, particularly in irradiated human cell lines (Fig. 3D, right panel).

Defects in postnatal growth, reproduction, and survival in Wip1 null mice. While *Wip1* nullizygosity may have had some effect on embryonic development in males, a number of postnatal defects were observed in these males. $Wip1^{-/-}$ males

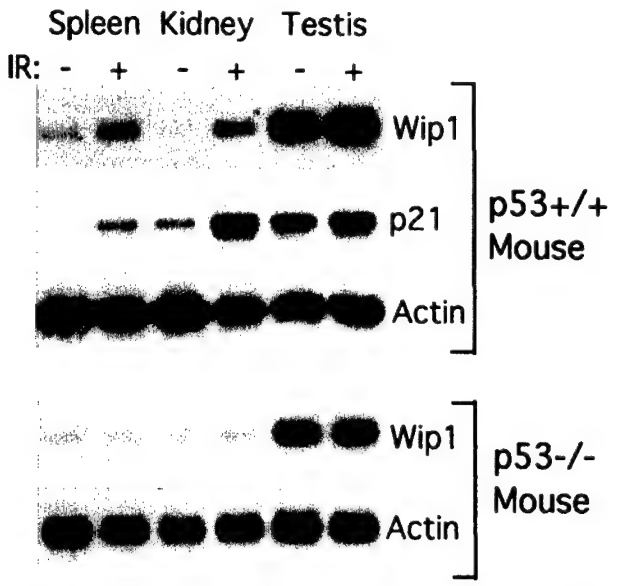

FIG. 2. p53-dependent induction of *Wip1* RNA expression by ionizing radiation (IR). RT-PCR assay on RNAs isolated from spleen, kidney, and testis of unirradiated and ionizing radiation-treated (10 Gy, 6 h) $p53^{+/+}$ and $p53^{-/-}$ mice. *Wip1*, p21, and actin primers were used to amplify 2 μg of total RNA for 25 cycles. Note the radiation induction of *Wip1* mRNA in spleen and kidney from $p53^{+/+}$ mice but not from $p53^{-/-}$ mice.

were sometimes runted as pups and were significantly smaller than their $Wip1^{+/-}$ and $Wip1^{+/+}$ siblings, which invariably appeared normal (Fig. 4A). $Wip1^{-/-}$ females did not exhibit this reduced body size. Mean body mass for 2- to 6-month-old $Wip1^{-/-}$ males was 21.6 g, whereas age-matched $Wip1^{+/+}$ males averaged 28.1 g. The difference between the $Wip1^{-/-}$ and $Wip1^{+/+}$ males was significant by *t* test ($P < 0.0001$). Mean body masses of 2- to 6-month-old $Wip1^{-/-}$ females and their $Wip1^{+/+}$ counterparts were 22.7 and 21.9 g, respectively, indicating no significant differences among the female genotypes ($P = 0.54$).

Gross examination of the organ systems of $Wip1^{-/-}$ animals did not reveal overt morphological differences in structure and size compared to $Wip1^{+/-}$ and $Wip1^{+/+}$ animals except that the male reproductive organs of the $Wip1^{-/-}$ males were often dramatically smaller than those of their wild-type and heterozygous counterparts (Fig. 4B). This was particularly true of the testes, which in the adult $Wip1^{-/-}$ males had an average mass of 64 mg, versus 110 mg for the $Wip1^{+/-}$ and $Wip1^{+/+}$ males. This difference was highly significant by *t* test ($P < 0.0001$). The reduced testis masses were not due solely to the reduced body masses of the $Wip1^{-/-}$ males, as even $Wip1^{-/-}$ males of normal weight often had testes of reduced size.

As might be expected, fertility in the $Wip1^{-/-}$ males was reduced. Four $Wip1^{+/+}$ and 16 $Wip1^{-/-}$ males mated to wild-type females produced an average of 20.0 and 6.0 offspring, respectively, over a period of 5 months. Seven of 16 $Wip1^{-/-}$ males produced no offspring but did generate postcoital vaginal plugs in the females, indicating that the infertile *Wip1* males were capable of mating. Other $Wip1^{-/-}$ males produced infrequent small litters, and a few produced litters at the same size and frequency as wild-type males. $Wip1^{+/-}$ males and $Wip1^{-/-}$ females demonstrated normal levels of fertility.

Another occasional observation was the presence of ulcerated skin lesions in approximately 5% of the $Wip1^{-/-}$ mice (Fig. 4C). These particular lesions were never observed in the $Wip1^{+/-}$ and $Wip1^{+/+}$ littermates. In addition, over 25% of the older null animals exhibited fluid-filled neck abscesses. The persistence of these skin lesions and abscesses was suggestive of an immune defect in the $Wip1^{-/-}$ mice.

Cohorts of $Wip1^{-/-}$, $Wip1^{+/-}$, and $Wip1^{+/+}$ mice were monitored for longevity over a period of 24 months. $Wip1^{-/-}$ male animals tended to appear less robust over their life span and showed a much higher incidence of spontaneous deaths compared to their $Wip1^{-/-}$ female and $Wip1^{+/-}$ and $Wip1^{+/+}$ littermates (Fig. 5). Only 3 of 20 $Wip1^{-/-}$ males survived to 2 years of age, whereas 15 of 17 of their $Wip1^{-/-}$ female littermates survived to 2 years of age. A log rank nonparametric survival test indicated that this difference was highly significant ($P < 0.0001$). In contrast to the $Wip1^{-/-}$ males, the $Wip1^{-/-}$ females had a survival rate similar to that of wild-type mice of the same background. Moreover, $Wip1^{+/-}$ males and females did not differ significantly in longevity from wild-type mice, as confirmed by the log rank test ($P > 0.5$). The cause of early deaths for the $Wip1^{-/-}$ males could not be determined directly, but cancers were virtually never observed in these animals, suggesting that nonneoplastic mechanisms might have been the more proximal causes of the deaths.

Organ histopathology in Wip1 null mice. The reduced size of the $Wip1^{-/-}$ male reproductive organs prompted a closer examination of the histopathology of these organs. Wip1 null testes often exhibited moderate or extensive degeneration of the seminiferous tubules, with extensive vacuolization, loss of normal cellular architecture, and, in the worst examples, absence of mature spermatozoa (Fig. 6A). However, in all cases examined there were clearly round and elongating spermatids, confirming that they had undergone meiosis and initiated terminal differentiation. Extensive cell death appears to be occurring within the germ cells, as marked by the presence of pycnotic nuclei.

The degeneration of the seminiferous epithelium suggests an inability to maintain spermatogenesis over time in the Wip1 null animals. The epididymis of the $Wip1^{-/-}$ male often exhibited atrophy as well, showing irregular tubules with abnormal architecture and an absence of spermatozoa, in contrast to the epididymi from wild-type mice, which were usually packed with spermatozoa (Fig. 6B). Thus, the diminished fertility of the $Wip1^{-/-}$ males is likely to be a result of the reduced number of spermatozoa produced by the null testes and defects in the epididymi.

Earlier gross examination revealed evidence of splenic enlargement in some of the 8- to 11-month-old *Wip1* null male and female animals, with spleen weights of 300 to 700 mg compared to the normal 100-mg spleens usually observed in age-matched wild-type animals. Histological comparison of the lymphoid organs of the $Wip1^{-/-}$ and $Wip1^{+/+}$ mice revealed that the lymph nodes, spleen, and bone marrow of the null animals often exhibited a pronounced myeloid and plasmacytic hyperplasia. In some cases the splenic hyperplasia was accompanied by loss of normal splenic architecture (Fig. 6C). In wild-type spleens, the white pulp regions were clearly demar-

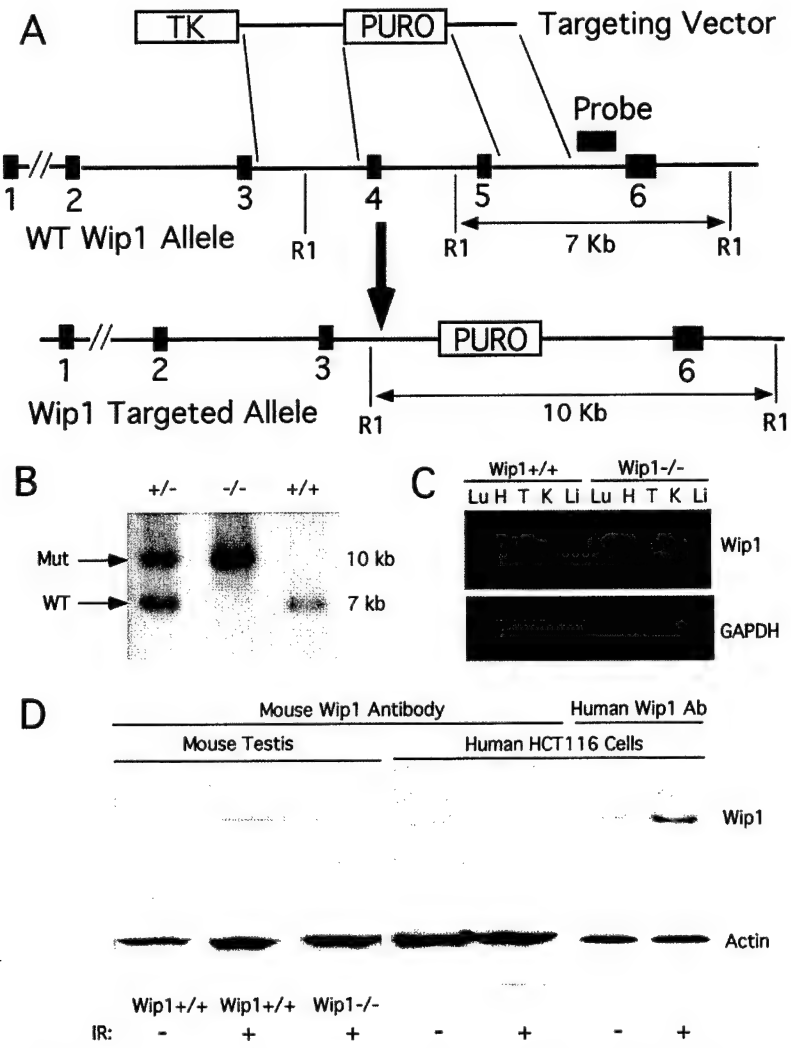

FIG. 3. Gene targeting of the *Wip1* allele and inactivation of Wip1 expression. (A) Gene targeting strategy for *Wip1* inactivation. Targeting deletes highly conserved domains in exons 4 and 5 and replaces them with a puromycin marker cassette. (B) Southern blot analysis confirming correct *Wip1* targeting in three offspring of *Wip1* heterozygote crosses. *Eco*RI cleavage of tail DNA and hybridization with the *Wip1* flanking probe (see panel A) generate a diagnostic 7-kb wild-type (WT) DNA fragment or a 10-kb mutant-specific DNA fragment. (C) Northern blot hybridization showing characteristic *Wip1* messages in the wild-type tissues and the absence of intact *Wip1* message in the *Wip1* null tissues. The five lanes to the left are from $Wip1^{+/+}$ tissues, while the right five lanes are from $Wip1^{-/-}$ tissues. Mouse tissue RNAs are from lung (Lu), heart (H), testis (T), kidney (K), and liver (Li). (D) Western blot analysis of Wip1 proteins in $Wip1^{-/-}$ and $Wip1^{+/+}$ testes and in normal human cell lines with murine-specific and human-specific Wip1 antibodies. Upper left panel shows that irradiated testes from $Wip1^{+/+}$ mice express high levels of the appropriately sized Wip1 protein, while irradiated testes from $Wip1^{-/-}$ mice express no apparent Wip1 protein when probed with a mouse Wip1 antibody. The upper middle panel indicates that human Wip1 is not recognized by the mouse-specific antibody, while the upper right panel shows that a human Wip1-specific antibody recognizes increased levels of Wip1 in irradiated human cells. The lower panels show loading control blots utilizing an antiactin antibody.

cated from the surrounding red pulp, whereas in the $Wip1^{-/-}$ sections, the white pulp regions were reduced in size and poorly demarcated from the red pulp regions due to infiltration by other cell types (Fig. 6C). No germinal centers could be identified in the white pulp, though prominent hematopoiesis was seen in the red pulp. The lymph nodes in some $Wip1^{-/-}$ mice also exhibited hyperplasia, accompanied by cellular infiltration with macrophages, neutrophils, and eosinophils. Bone marrow also showed evidence of myeloid hyperplasia in some of the older $Wip1^{-/-}$ mice. The thymus of some older *Wip1* null mice also showed a reduction in size and a loss of normal medullary-cortical architecture.

A number of organs in the $Wip1^{-/-}$ mice exhibited increased levels of inflammation, particularly in those animals exhibiting skin ulcerations. These lesions showed extensive pyogranulomatous inflammation, infiltrating mast cells, epidermal proliferation, acanthosis, and hyperkeratosis. Inflammation in organs of $Wip1^{+/-}$ and $Wip1^{+/+}$ animals was observed at relatively minimal levels.

Pathogen susceptibility of *Wip1* null mice. The increased presence of inflammation, skin ulcerations, and abnormal lymphoid histopathology suggested defects in immunocompetence in the $Wip1^{-/-}$ mice. To more directly test this possibility, we challenged four $Wip1^{-/-}$ male mice and five $Wip1^{+/-}$ male

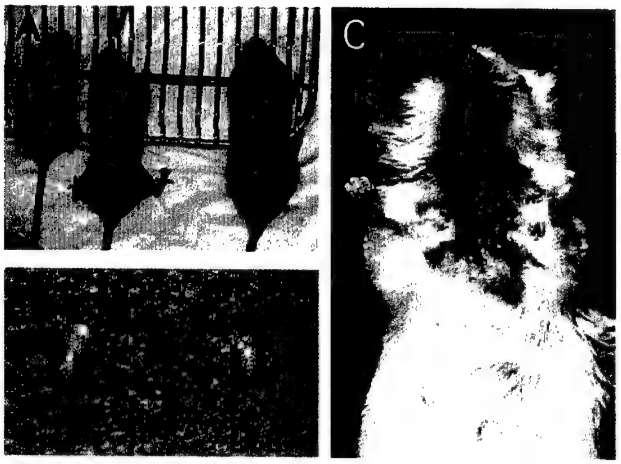

FIG. 4. Morphological alterations in *Wip1* null males. (A) $Wip1^{-/-}$ mice were sometimes runted. The two smaller animals on the left are $Wip1^{-/-}$ male littermates along with a wild-type male littermate at 5 weeks of age. (B) $Wip1^{-/-}$ testes are often reduced in size even in normal-sized $Wip1^{-/-}$ males. The testis on the left is from a $Wip1^{+/+}$ male, and the testis on the right is from a normal-sized $Wip1^{-/-}$ male. (C) $Wip1^{-/-}$ animals are more susceptible to ulcerated skin lesions. Shown is a $Wip1^{-/-}$ female mouse with an ulcerated lesion on its underside. This type of lesion has not been observed in wild-type animals in our colony.

mice with 1 LD_{50} of a mouse-adapted pathogenic influenza virus according to previous protocols (14). The virus-infected mice were then monitored for 21 days. All of the infected mice of both genotypes showed significant morbidity and body weight loss by 7 days postinfection. All four $Wip1^{-/-}$ males died by 11 days postinfection, while four of the five $Wip1^{+/-}$ males recovered from the virus and appeared healthy at 12 to 15 days postinfection (Fig. 7A). This difference in mortality was statistically significant by log rank analysis ($P = 0.013$).

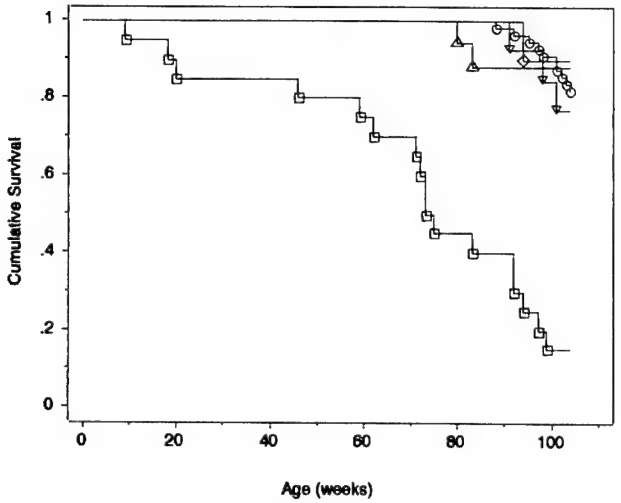

FIG. 5. Longevity of $Wip1^{-/-}$ males is dramatically reduced. Kaplan-Meier plots of $Wip1^{-/-}$ males (squares, $n = 20$), $Wip1^{-/-}$ females (triangles, $n = 17$), $Wip1^{+/-}$ males (diamonds, $n = 10$), $Wip1^{+/-}$ females (inverted triangles, $n = 13$), and $Wip1^{+/+}$ mice (circles, $n = 55$) are shown. Note that only the $Wip1^{-/-}$ males have a significantly reduced longevity in comparison to wild-type mice.

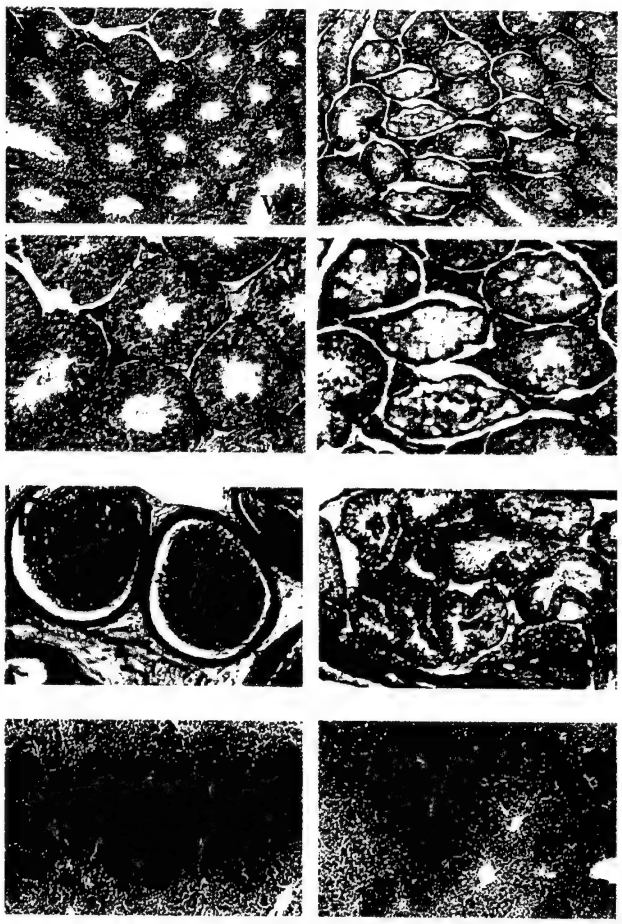

FIG. 6. Histopathology of $Wip1^{-/-}$ and $Wip1^{+/+}$ male reproductive organs and spleens. (A) Stained cross sections of representative $Wip1^{+/+}$ testis (left two panels at different magnifications) and $Wip1^{-/-}$ testis (right two panels) show dramatic differences in the architecture of the seminiferous tubules. (B) Stained cross section of representative $Wip1^{+/+}$ epididymis (left panel) and $Wip1^{-/-}$ epididymis (right panel). The tubules of the wild-type epididymis show normal structure and are filled with spermatozoa, whereas the null epididymis tubules appear atrophied and devoid of spermatozoa. (C) Absence of *Wip1* affects splenic architecture. Left panel shows a spleen cross section from an 8-month-old wild-type mouse, while the right panel shows a cross section from an 8-month-old $Wip1^{-/-}$ spleen. Note the atrophied and disorganized state of the splenic white pulp in the $Wip1^{-/-}$ spleen.

Thus, $Wip1^{-/-}$ mice do appear to be immunologically deficient, as measured by the ability to resolve an infection by a lethal pathogen.

Defects in *Wip1* null T- and B-cell responses. The increased susceptibility of the *Wip1* null animals to a lethal pathogen prompted an examination of their T- and B-cell populations and functions. Fresh, uncultured spleen cells from 3- to 6-month-old $Wip1^{-/-}$ and $Wip1^{+/+}$ male mice were examined by flow cytometry for the presence of a variety of lymphoid cell surface antigens, including $CD19^+$ and $CD19^+/IgG^+$ (for B cells) and $CD3^+$, $CD4^+$, and $CD8^+$ (for T cells). $CD19^+$ and $CD19^+/IgG^+$ B cells were not significantly different in number between $Wip1^{-/-}$ and $Wip1^{+/+}$ animals (Fig. 7B). Moreover, $CD3^+$ T cell numbers were similar in both genotypes. However, $CD4^+$ T cells were increased in number in $Wip1^{-/-}$ mice,

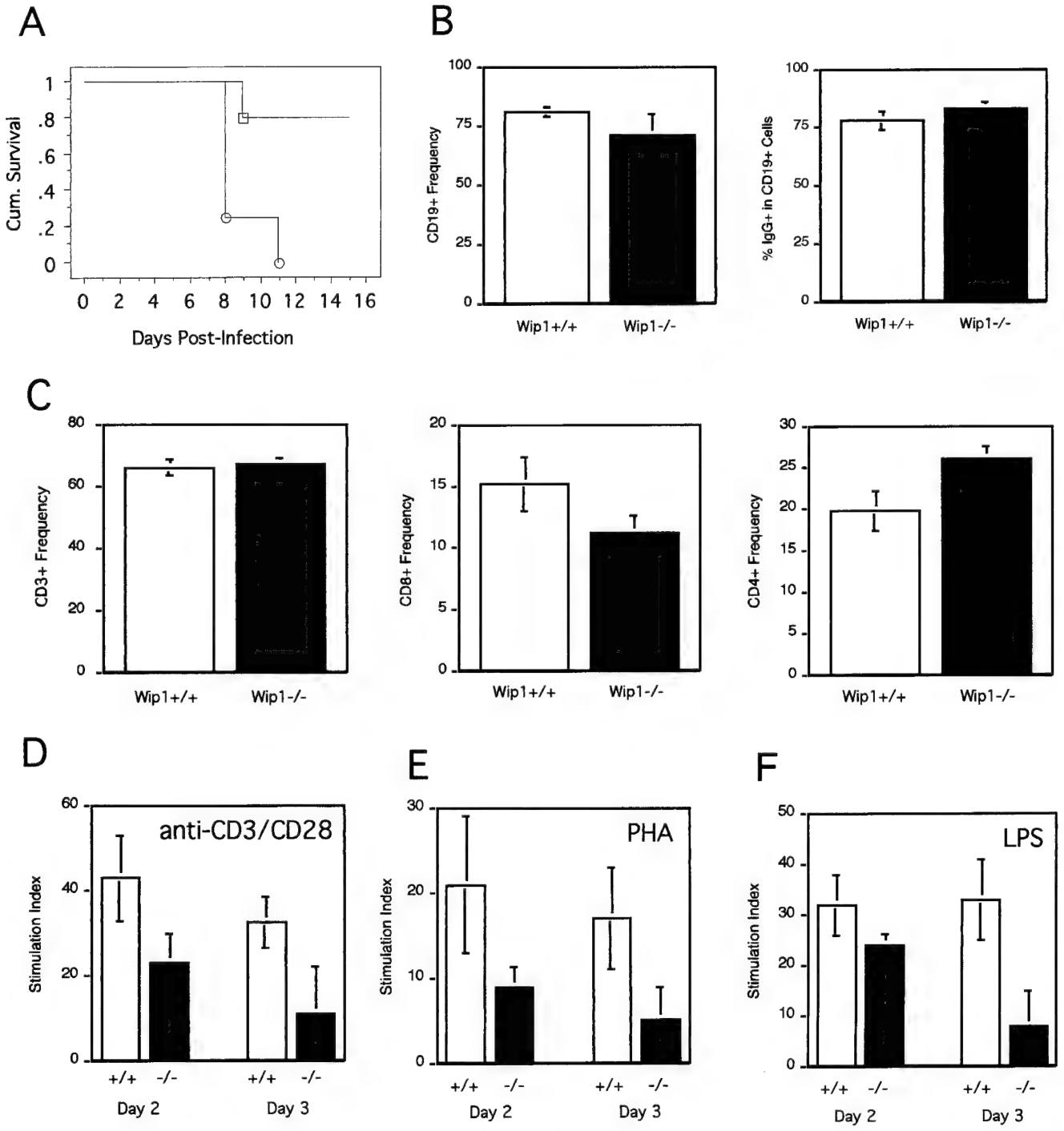

FIG. 7. Pathogen response and T- and B-cell function in *Wip1*$^{-/-}$ mice. (A) Kaplan-Meier survival plot of four *Wip1*$^{-/-}$ and five *Wip1*$^{+/-}$ males infected with one LD_{50} of mouse-adapted influenza virus. Circles represent *Wip1*$^{-/-}$ survival, while squares show *Wip1*$^{+/-}$ survival. (B) Quantitation by flow cytometry of $CD19^+$, $CD19^+/IgG^+$ B cells. (C) $CD3^+$, $CD4^+$, and $CD8^+$ T cells in *Wip1*$^{+/+}$ and *Wip1*$^{-/-}$ male mice. Note the increased numbers of $CD4^+$ T cells and decreased numbers of $CD8^+$ T cells in *Wip1*$^{-/-}$ animals. (D) T-cell proliferative responses to antigenic stimulation. Note the significantly decreased proliferative response of the *Wip1*$^{-/-}$ T cells to anti-CD3 plus anti-CD28. (E) T-cell proliferative responses to mitogenic stimulation. Note the significantly decreased proliferative response of the *Wip1*$^{-/-}$ T cells to the mitogen PHA. (F) B-cell proliferative response to mitogenic stimulation. The *Wip1*$^{-/-}$ B cells show a significantly reduced proliferative response to the mitogen LPS.

and $CD8^+$ T cells were decreased in number in *Wip1*$^{-/-}$ mice (Fig. 7C).

The T- and B-cell proliferative responses to mitogenic stimulation were further examined. Stimulation of splenic T cells with anti-CD3 and -CD28 elicited a reduced proliferative response in the *Wip1*$^{-/-}$ cells compared to the *Wip1*$^{+/+}$ cells at both 2 and 3 days poststimulation, indicating defects in normal T-cell receptor-mediated signaling (Fig. 7D). Addition of the

polyclonal T-cell mitogen PHA to splenocytes also resulted in a dramatic reduction in response by the *Wip1*$^{-/-}$ T cells compared to their *Wip1*$^{+/+}$ counterparts (Fig. 7E). Finally, addition of the B-cell mitogen LPS evoked a less robust proliferative response by *Wip1*$^{-/-}$ B cells, suggesting that both B and T cells in the *Wip1* null mice have partially compromised function (Fig. 7F). When these T- and B-cell functional assays were performed on splenocytes from older *Wip1*$^{-/-}$ and *Wip1*$^{+/+}$ mice, the results were similar (data not shown).

Fibroblasts from Wip1 null embryos exhibit multiple cell cycle defects. To assess whether the absence of *Wip1* had any effect on other cell growth phenotypes, we isolated fibroblasts from midgestation *Wip1*$^{-/-}$ and *Wip1*$^{+/+}$ embryos and cultured them under standard conditions. Soon after plating the *Wip1*$^{-/-}$ MEFs, it became obvious that they grow much more slowly than their *Wip1*$^{+/+}$ counterparts. Growth curve analyses of *Wip1*$^{-/-}$ and *Wip1*$^{+/+}$ MEFs confirmed that the proliferation rates of early-passage *Wip1*$^{-/-}$ MEFs were substantially retarded compared to *Wip1*$^{+/+}$ MEFs (Fig. 8A). Thirteen days after plating three lines of 7.5×10^5 *Wip1*$^{-/-}$ early-passage MEFs, they grew to a mean of 2.5×10^6 cells per plate, versus a mean of 5.5×10^6 cells per plate for three lines of *Wip1*$^{+/+}$ cells.

Flow cytometric analysis of dividing *Wip1*$^{-/-}$ and *Wip1*$^{+/+}$ MEFs for DNA content and BrdU labeling indicated a decreased percentage of cells in S phase and mitosis (Table 1). The G_2/M ratio of *Wip1*$^{-/-}$ cells was over threefold greater than that of the *Wip1*$^{+/+}$ MEFs, suggesting a block in entering mitosis in the *Wip1* null MEFs. Colony formation following plating at low density was also significantly reduced in the *Wip1*$^{-/-}$ MEFs (Fig. 8B).

Continued passaging of the *Wip1*$^{-/-}$ MEFs led to a rapid cessation of division, suggestive of a premature senescence. By passage 13, the *Wip1*$^{-/-}$ MEFs had essentially stopped dividing, while their *Wip1*$^{+/+}$ counterparts were still dividing at a robust rate (Fig. 8C). The morphology of these proliferatively inactivated *Wip1*$^{-/-}$ fibroblasts was similar to that of senescent normal fibroblasts, with a flattened, vacuolated, enlarged appearance. Whether or not the *Wip1*$^{-/-}$ MEFs are truly senescent remains uncertain, but it is clear that they have a greatly reduced number of population doublings in culture compared to their *Wip1*$^{+/+}$ counterparts.

To determine whether *Wip1* null MEFs maintained a normal G_1 DNA damage checkpoint, we treated *Wip1*$^{+/+}$, *Wip1*$^{-/-}$, and p53$^{-/-}$ MEFs with 5 Gy of ionizing radiation (IR) and monitored their G_1 arrest checkpoints at 24 h after irradiation. Not surprisingly, p53$^{-/-}$ MEFs showed no defect in S-phase entry (as measured by BrdU incorporation) compared to unirradiated p53$^{-/-}$ MEFs 24 h after IR treatment (Fig. 8D). At 24 h post-IR, both *Wip1*$^{-/-}$ and *Wip1*$^{+/+}$ MEFs showed a strong G_1 arrest phenotype, though the *Wip1*$^{-/-}$ MEFs consistently showed a more robust G_1 arrest than their *Wip1*$^{+/+}$ counterparts (Fig. 8D). These experiments indicate that *Wip1* null cells do not have a defect in initiating G_1 arrest in response to DNA damage.

The decreased cell cycle progression and more robust DNA damage-induced G_1 arrest phenotype of the *Wip1*$^{-/-}$ MEFs suggested the possibility that they may have higher levels of activated p53. This would be consistent with the inhibitory effects of Wip1 on the p53-activating p38 MAP kinase (25). To assess this possibility, we determined p53 levels in dividing *Wip1*$^{+/+}$ and *Wip1*$^{-/-}$ MEFs by Western blot analysis using a p53-specific antibody. p53 levels were similar in both types of MEFs, indicating that p53 is not produced at higher levels and does not have higher stability in *Wip1*$^{-/-}$ MEFs (Fig. 8E).

The relative activity of p53 in *Wip1*$^{+/+}$ and *Wip1*$^{-/-}$ MEFs was measured by determining expression levels of a p53 target gene, p21 $^{WAF1/CIP1}$, and phosphorylation of serine 15, markers for activated p53 (4, 22). *Wip1*$^{-/-}$ MEFs consistently showed higher levels of p21 protein and p53 phosphorylated serine 15 than *Wip1*$^{+/+}$ MEFs, suggesting that p53 functional activity was higher in these cells (Fig. 8E and F).

DISCUSSION

The *Wip1* gene has been shown to be a serine/threonine phosphatase inducible by UV and ionizing radiation in a p53-dependent manner in cells in culture (5, 25). While the function of *Wip1* is presently unclear, its p53 responsiveness (5) and association with p38 MAP kinase (25) suggest that it may play an important role in cell signaling in response to cellular stress. Our finding that *Wip1* mRNA is expressed in all examined tissues of the mouse is consistent with the hypothesis that Wip1 plays a global role in signaling in all cell types. Moreover, the demonstration that Wip1 is induced by ionizing radiation in multiple mouse tissues only when p53 is present confirms that it is a bona fide p53 target gene. The mechanism through which p53 induces *Wip1* RNA expression is not known, since a consensus p53 response element has not been identified in the *Wip1* promoter region (2), but we have observed that the *Wip1* promoter does confer p53 inducibility in cell transfection assays (data not shown).

While *Wip1* mRNA expression appears to be ubiquitous in all mouse tissues, the testes contain extremely high RNA levels. In situ hybridization experiments on testis sections revealed that Wip1 was expressed in spermatogenic cells, with its expression first detected in late-stage pachytene spermatocytes just prior to the completion of meiosis. The highest expression levels of Wip1 are in the postmeiotic round spermatid compartment. Thus, the expression of Wip1 correlates with the final stages of meiosis, and it may play a role in regulating the meiosis I and II divisions.

The high level of Wip1 expression in round spermatids suggests that it plays a role in inhibiting further cell cycles, thus maintaining the haploid state. Since there are round and elongating spermatids in the seminiferous tubules of *Wip1* null animals, this suggests that Wip1 is not essential for the completion of meiosis. However, a more detailed analysis of the cell cycle state of the haploid spermatids in these animals might highlight a subtle meiotic defect. Alternatively, there could be a closely related family member that is compensating for its function in male germ cells.

The defects in male fertility of the *Wip1* null mice are probably due to the dual effects on the spermatogenic cells and the epididymi, similar to what was observed with the estrogen receptor alpha knockout mouse, whose mutation affected both the somatic cells of the testis and the epididymi (10). The fact that many of the *Wip1*$^{-/-}$ male mice have smaller reproductive organs and reduced fertility suggests that this gene plays a major role in development of the male reproductive structures.

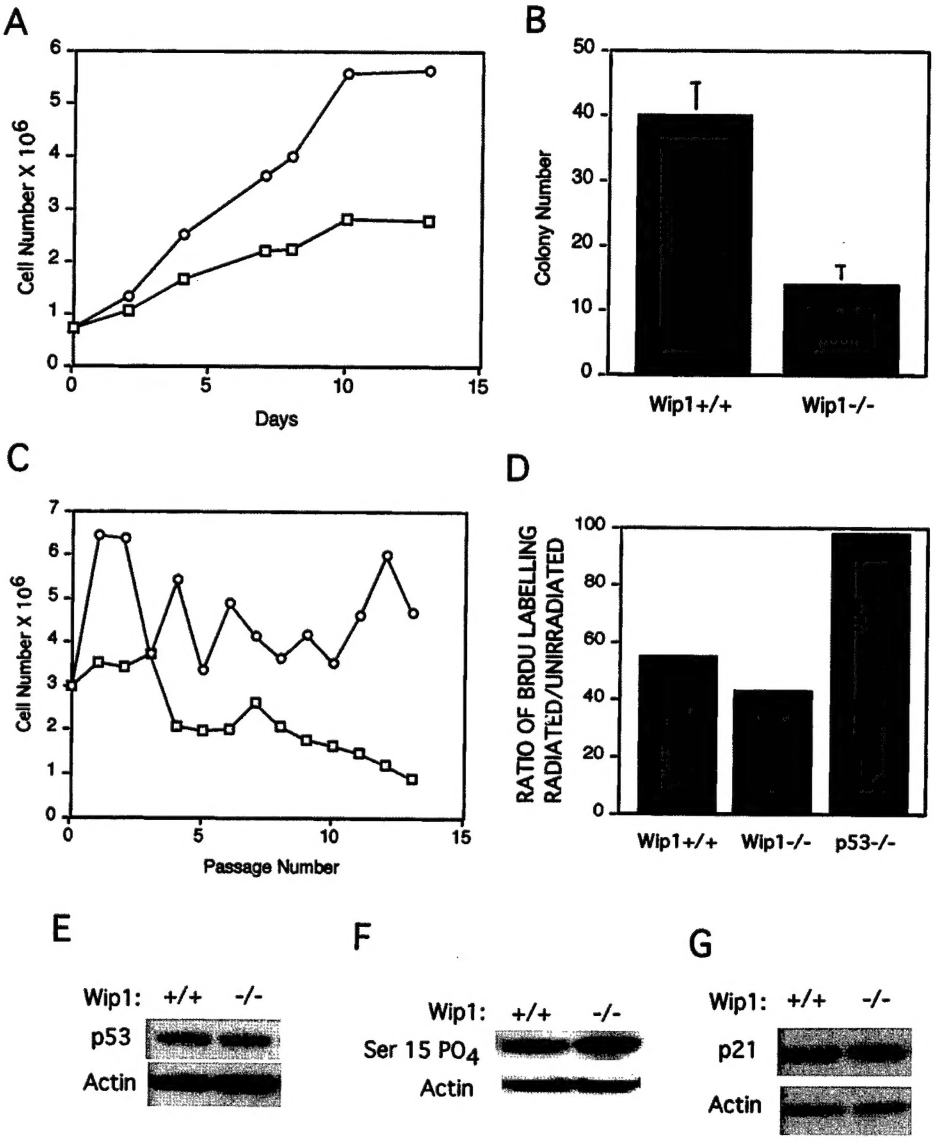

FIG. 8. Growth phenotypes of $Wip1^{+/+}$ and $Wip1^{-/-}$ embryo fibroblasts. (A) Growth of 7.5×10^5 early-passage MEFs derived from $Wip1^{-/-}$ and $Wip1^{+/+}$ embryos and monitored for growth over a period of 13 days. Representative growth curves are shown for $Wip1^{+/+}$ (circles) and $Wip1^{-/-}$ (squares) MEFs. The $Wip1^{-/-}$ MEFs consistently showed slower growth kinetics. (B) Low-density colony formation assay, in which 10,000 $Wip1^{+/+}$ or $Wip1^{-/-}$ MEFs were plated on 100-mm tissue culture dishes, incubated for 2 weeks, and then fixed, stained, and counted for colonies with more than 30 cells. (C) Long-term passaging of $Wip1^{+/+}$ and $Wip1^{-/-}$ MEFs. Equal numbers of $Wip1^{+/+}$ (circles) and $Wip1^{-/-}$ (squares) cells were passaged every 3 days over 13 passages. Early during the passaging, $Wip1^{-/-}$ MEFs reached a terminal nondividing state reminiscent of senescence, whereas wild-type MEFs continued to divide rapidly through 13 passages. (D) G_1 arrest response in $Wip1^{+/+}$, $Wip1^{-/-}$, and $p53^{-/-}$ MEFs. $Wip1^{+/+}$, $Wip1^{-/-}$, and $p53^{-/-}$ MEFs were synchronized in G_1, and half of the cells of each genotype were treated with 5 Gy of ionizing radiation. After BrdU addition, cells were harvested at 24 h after irradiation and subjected to flow cytometry for DNA content and BrdU labeling. The ratio of BrdU-labeled cells in treated versus untreated MEFs for each genotype was determined. Note that $p53^{-/-}$ control MEFs are unaffected by irradiation, as expected. (E) p53 levels in early-passage $Wip1^{+/+}$ and $Wip1^{-/-}$ MEFs. p53 protein levels in $Wip1^{+/+}$ and $Wip1^{-/-}$ MEFs were determined by Western blot analysis with a p53-specific polyclonal antibody. (F) Phosphorylation of p53 serine 15 in $Wip1^{+/+}$ and $Wip1^{-/-}$ early-passage MEFs, determined by Western blot analysis using a polyclonal antibody specific for phosphorylated serine 15, following 5 Gy of ionizing radiation. (G) p21 $^{WAF1/CIP1}$ protein levels in early-passage $Wip1^{+/+}$ and $Wip1^{-/-}$ MEFs, determined by Western blot analysis using a polyclonal antibody specific for p21.

However, the precise mechanisms by which *Wip1* could influence this process remain to be elucidated.

The viability of $Wip1^{-/-}$ males and females indicates that Wip1 is not essential for embryonic development, yet the reduced ratio of $Wip1^{-/-}$ male offspring suggests that Wip1 may play a subtle role in influencing development of the males. Moreover, the $Wip1^{-/-}$ males exhibit a number of pleiotropic postnatal defects, such as runting, reproductive defects, and reduced longevity, that are not exhibited by the *Wip1*-deficient females. The reproductive deficiencies of the $Wip1^{-/-}$ males

TABLE 1. Cell cycle analysis of *Wip1*$^{+/+}$ and *Wip1*$^{-/-}$ MEFs

Cell cycle phase	% of MEFs	
	Wip1$^{+/+}$	*Wip1*$^{-/-}$
G_1	56.9	48.7
S	20.5	16.8
G_2/M	29.6	36.9
M	1.7	0.7
(G_2 to M ratio)	(17.4)	(52.7)

are presumably related to the aberrant architecture seen in the seminiferous tubules and epididymi, leading to the paucity of mature spermatozoa seen in many of the seminiferous tubules and epididymi. These defects in spermatogenesis contrast to those observed in p53 null mice, whose testes exhibited multinucleated giant cells suggestive of a degenerative syndrome resulting from the inability of the tetraploid primary spermatocytes to complete meiotic division (19).

The mechanisms of runting and reduced longevity seen in the null males are less clear, but may be a result of male hormone deficiencies accompanying the reduction in reproductive organ development. A complete age-related analysis of the hormonal status of these animals should shed light on the contribution of endocrinological defects to these phenotypes. The normal phenotypic appearance and longevity of the female *Wip1*$^{-/-}$ mice indicate that Wip1 is relatively dispensable for normal prenatal and postnatal function, though there may be changes in immune function which do not affect longevity.

Several observations indicate that the *Wip1*$^{-/-}$ animals have immune defects. These include the presence of ulcerated skin lesions in some animals, the disorganized and hyperplastic architecture in the lymphoid organs, the increased inflammation observed in normal organs, and the defects in the proliferative responses of T and B cells to antigenic and mitogenic stimulation. The most compelling evidence for an immunological defect was provided by the increased mortality of influenza virus-challenged *Wip1*$^{-/-}$ mice. The reduced T- and B-cell responses may partially explain the increase in the inflammatory response, since a defect in one part of the adaptive immune system may result in compensation by innate immune system components, including the neutrophils and macrophages. Whether these potential defects in immune function are related to the decreased longevity of the null males is unclear, since some of the older null females also show evidence of inflammatory lesions and hyperplastic disorganization of lymphoid structures. The hyperplasias and atrophic disorganization observed in the *Wip1* null spleens were not preneoplastic, in contrast to the hyperplasias observed in p53 null spleens (27).

While T and B cells isolated from *Wip1*$^{-/-}$ animals have defects in proliferation, *Wip1*$^{-/-}$ embryo fibroblasts show even more profound deficits in growth in vitro . *Wip1* null MEFs show low proliferation rates and enter S phase and especially mitosis less frequently than normal MEFs. Not only do *Wip1*$^{-/-}$ MEFs grow more slowly, but they seem to exhibit relatively few divisions prior to entering a senescence-like state. Thus, Wip1 is clearly an important component of cell cycle progression, at least in vitro. Why it does not seem to be equally important for cell division in the intact animal is unclear, but there may be compensatory pathways in vivo which mask the effects of Wip1 absence.

Based on early studies, Wip1 is likely to be an important component in the response to cell stress induced by radiation. Fiscella et al. (5) have shown that radiation induces increased *Wip1* expression in a p53-dependent manner, and Takekawa et al. (25) have shown that Wip1 can inhibit p38 MAP kinase through dephosphorylation of a UV-activated threonine residue. We have demonstrated here that ionizing radiation induces a robust G_1 arrest in *Wip1*$^{-/-}$ MEFs. The slight enhancement of the G_1 arrest in *Wip1* null cells compared to normal cells is consistent with the data of Takekawa et al. (25) indicating that the presence of Wip1 may inhibit the activated status of p53 through p38 MAP kinase deactivation.

Unstressed *Wip1*$^{-/-}$ MEFs divide much more slowly than their normal counterparts, as indicated by growth curves, long-term passaging, and flow cytometric analyses. These results indicate that Wip1 plays an important cell cycle regulatory role. *Wip1*$^{-/-}$ MEFs appear to be particularly compromised in the mitotic transition, as *Wip1*$^{-/-}$ cells have a much higher G_2/M ratio than normal cells. This suggests that the phosphatase activity of Wip1 may target proteins involved in mediating mitosis. However, we have provided evidence that at least some of the decreased cell cycle progression in *Wip1* null MEFs may be a result of a more activated p53 in these cells. This may be due to the effects of Wip1 in inactivating the p53-specific p38 MAP kinase (13), although action of Wip1 on other p53 effectors cannot be ruled out. The elucidation of such Wip1 targets will be of considerable importance for our understanding of its role in stress response and cell cycle control. Moreover, the availability of viable *Wip1* null cells and animals should provide additional tools for understanding the function of Wip1 at both the cellular and the organismal level.

ACKNOWLEDGMENTS

We thank Jerrold Ward for histopathological analyses of some of the *Wip1*$^{-/-}$ spleens and thymic tissues. We thank Eunice Varghese and Chao-Ling Wu for technical assistance and Marco Schito for helpful discussions.

This work was supported by a grant from the National Cancer Institute (CA54897) to L.A.D.

REFERENCES

1. **Bulavin, D. V., N. D. Tararova, N. D. Aksenov, V. A. Pospelov, and T. V. Pospelova.** 1999. Deregulation of p53/p21Cip1/Waf1 pathway contributes to polyploidy and apoptosis of E1A+cHa-ras transformed cells after gamma-irradiation. Oncogene **18**:5611–5619.
2. **Choi, J., E. Appella, and L. A. Donehower.** 2000. The structure and expression of the murine wild-type p53-induced phosphatase 1 (Wip1) gene. Genomics **64**:298–306.
3. **Cohen, P.** 1989. The structure and regulation of protein phosphatases. Annu. Rev. Biochem. **58**:453–508.
4. **el-Deiry, W. S., T. Tokino, V. E. Velculescu, D. B. Levy, R. Parsons, J. M. Trent, D. Lin, W. E. Mercer, K. W. Kinzler, and B. Vogelstein.** 1993. WAF1, a potential mediator of p53 tumor suppression. Cell **75**:817–825.
5. **Fiscella, M., H. Zhang, S. Fan, K. Sakaguchi, S. Shen, W. E. Mercer, G. F. Vande Woude, P. M. O'Connor, and E. Appella.** 1997. Wip1, a novel human protein phosphatase that is induced in response to ionizing radiation in a p53-dependent manner. Proc. Natl. Acad. Sci. USA **94**:6048–6053.
6. **Freshney, I.** 1983. Culture of animal cells: a manual of basic technique, p. 99–118. Alan R. Liss, Inc., New York, N.Y.
7. **Giaccia, A. J., and M. B. Kastan.** 1998. The complexity of p53 modulation: emerging patterns from divergent signals. Genes Dev. **12**:2973–2983.
8. **Greenblatt, M. S., W. P. Bennett, M. Hollstein, and C. C. Harris.** 1994. Mutations in the p53 tumor suppressor gene: clues to cancer etiology and molecular pathogenesis. Cancer Res. **54**:4855–4878.
9. **Harvey, M., A. T. Sands, R. S. Weiss, M. E. Hegi, R. W. Wiseman, P.**

Pantazis, B. C. Giovanella, M. A. Tainsky, A. Bradley, and L. A. Donehower. 1993. In vitro growth characteristics of embryo fibroblasts isolated from p53-deficient mice. Oncogene **8**:2457–2467.

10. **Hess, R. A., D. Bunick, K. H. Lee, J. Bahr, J. A. Taylor, K. S. Korach, and D. B. Lubahn.** 1997. A role for oestrogens in the male reproductive system. Nature **390**:509–512.
11. **Ko, L. J., and C. Prives.** 1996. p53: puzzle and paradigm. Genes Dev. **10**:1054–1072.
12. **Levine, A. J.** 1997. p53, the cellular gatekeeper for growth and division. Cell **88**:323–331.
13. **Lozano, G., and S. J. Elledge.** 2000. p53 sends nucleotides to repair DNA. Nature **404**:24–25.
14. **Mbawuike, I. N., H. R. Six, T. R. Cate, and R. B. Couch.** 1990. Vaccination with inactivated influenza A virus during pregnancy protects neonatal mice against lethal challenge by influenza A viruses representing three subtypes. J. Virol. **64**:1370–1374.
15. **Mumby, M. C., and G. Walter.** 1993. Protein serine/threonine phosphatases: structure, regulation, and functions in cell growth. Physiol. Rev. **73**:673–699.
16. **Ramirez-Solis, R., J. Rivera-Perez, J. D. Wallace, M. Wims, H. Zheng, and A. Bradley.** 1992. Genomic DNA microextraction: a method to screen numerous samples. Anal. Biochem. **201**:331–335.
17. **Ramirez-Solis, R., A. C. Davis, and A. Bradley.** 1993. Gene targeting in embryonic stem cells. Methods Enzymol. **225**:855–878.
18. **Relyea, J. Miller, D. Boggess, and J. Sundberg.** 2000. Necropsy methods for laboratory mice: biological characterization of a new mutation, p. 57–89. *In* J. P. Sundberg and D. Boggess (ed.), Systematic. approach to evaluation of mouse mutations. CRC Press, Boca Raton, Fla.
19. **Rotter, V., D. Schwartz, E. Almon, N. Goldfinger, A. Kapon, A. Meshorer, L. A. Donehower, and A. J. Levine.** 1993. Mice with reduced levels of p53 protein exhibit the testicular giant-cell degenerative syndrome. Proc. Natl. Acad. Sci. USA **90**:9075–9079.
20. **Sambrook, J., E. F. Fritsch, and T. Maniatis.** 1989. Molecular cloning: a laboratory manual, p. 7.1–7.87. Cold Spring Harbor Laboratory Press, Cold Spring Harbor, N.Y.
21. **Sherr, C. J.** 1998. Tumor surveillance via the ARF-p53 pathway. Genes Dev. **12**:2984–2991.
22. **Siliciano, J. D., C. E. Canman, Y. Taya, K. Sakaguchi, E. Appella, and M. B. Kastan.** 1997. DNA damage induces phosphorylation of the amino terminus of p53. Genes Dev. **11**:3471–3481.
23. **Steele, R. J., A. M. Thompson, P. A. Hall, and D. P. Lane.** 1998. The p53 tumour suppressor gene. Br. J. Surg. **85**:1460–1467.
24. **Suckow, M. A., P. Danneman, and C. Brayton.** 2001. The laboratory mouse, p. 113–143. CRC Press, Boca Raton, Fla.
25. **Takekawa, M., M. Adachi, A. Nakahata, I. Nakayama, F. Itoh, H. Tsukuda, Y. Taya, and K. Imai.** 2000. p53-inducible wip1 phosphatase mediates a negative feedback regulation of p38 MAPK-p53 signaling in response to UV radiation. EMBO J. **19**:6517–6526.
26. **Vogelstein, B., D. Lane, and A. J. Levine.** 2000. Surfing the p53 network. Nature **408**:307–310.
27. **Ward, J. M., L. Tadesse-Heath, S. N. Perkins, S. K. Chattopadhyay, S. D. Hursting, and H. C. Morse III.** 1999. Splenic marginal zone B-cell and thymic T-cell lymphomas in p53-deficient mice. Lab. Investig. **79**:3–14.